Bacterial Cellulose as a new biomaterial for bioprosthetic heart valves

Master of Science Thesis

Mirthe Smeenk
4282299

Faculty of Biomedical Engineering

TU Delft

UNIVERSITÄT BERN

INSELSPITAL
UNIVERSITÄTSSPITAL BERN
HÔPITAL UNIVERSITAIRE DE BERNE

Bacterial Cellulose as a new biomaterial for bioprosthetic heart valves

Master of Science Thesis

Author:

Mirthe Smeenk

4282299

Date:

16^{th} of October, 2018

Programme:

Biomedical Engineering

Specialisation:

Biomaterials and Tissue Biomechanics

Supervisors:

Prof. Dr. Amir Zadpoor, Delft University of Technology

Dr. Iulian Apachitei, Delft University of Technology

Dr. Med. Paul Philipp Heinisch, University Hospital Bern

Silje Jahren, Msc., University of Bern

Prof. Dr. Dominik Obrist, University of Bern

On behalf of:

Delft University of Technology

Inselspital, University Hospital Bern

University of Bern, Switzerland

Abstract

As the population ages and the know-how of the medical field progresses, the number of surgical interventions is rapidly expanding. Heart valve replacement surgery is no exception to this phenomenon; every year 280 000 heart valve replacement surgeries are performed worldwide. Despite the success of heart valve replacement surgeries, various notable drawbacks hinder its advancement. Mechanical heart valves require anticoagulant therapy to reduce the risk of thromboembolisms, thereby also introducing anticoagulant-induced haemorrhage. Furthermore, the need for anticoagulant therapy makes the mechanical valve undesirable for woman who desire a pregnancy. Bioprosthetic heart valves suffer from structural valve deterioration and therefore need to be replaced after less than 15 years. Replacement surgery is dangerous, with an increased mortality rate of up to 20%. Furthermore, heart valve prosthetics do not allow for native cell tissue ingrowth, limiting their ability to self-repair and grow, the latter being of especially high importance in pediatric heart valve surgeries.

A promising new concept is the tissue engineered prosthetic heart valve, which would hypothetically remove the need for anticoagulent use, allow for self-repair and growth and increase the durability of heart valve prosthetics. The process of creating a Tissue Engineered Heart Valve (TEHV) is, however, complex, and an optimal scaffold is yet to be found.

Bacterial Cellulose (BC) is hypothesised to be a feasible scaffold and material for use in heart valve prostheses. BC is a biogenic polymer with a chemical structure not unlike collagen. The material is produced by, among others, the bacterium *Acetobacter Xylinus*. BC has been shown to have considerable mechanical strength and low thrombogenicity. Furthermore, a study in rat models has indicated no inflammatory or foreign body response to implanted cellulose. Bacterial cellulose is already successfully in use as wound dressing, and has been utilised to produce feasible vascular grafts. However, to the knowledge of the author, pure BC has not yet been used for the production of prosthetic heart valves.
BC has been cultured statically with a novel method of automatic medium exchange, and rotational with a specially designed rotation device.
The BC cultured with the novel method of automatic medium exchange, is more stable and stronger than patches cultured with the previous culturing protocol. However, BC cultured using the rotary device is unstable and fragile. The rotary culturing protocol needs to be improved in order to result in feasible BC tubes for the production of heart valves.

The BC shows strain levels slightly stiffer, but relatively similar to those of human pericardium. Furthermore, creep behaviour is, as with pericardium, insignificant under cyclic loading conditions.

More patches need to be cultured in order to increase the sample size, and thereby produce more conclusive results. The results already gathered in this master thesis research, show that BC material has promising mechanical characteristics, possibly rendering it a feasible option for the use in bioprosthetic heart valves.

Acknowledgments

First, I wish to thank Prof. Dr. Dominik Obrist for allowing me to write my thesis at the ARTORG Center for Biomedical Engineering Research. I have been able to work with the group's pulsatile flow-loops and other lab equipment. Professor Obrist has also provided resources for the construction of the rotary machine, and has provided valuable feedback and input throughout the project.
Secondly, I would like to thank Dr. med. Paul Phillip for supporting me and helping me in finding solutions to encountered problems.
Thirdly, I want to thank Silje Jahren for being willing to supervise me during my thesis. She was open for questions and willing to help when necessary.
Fourthly, a thank you goes out to my supervisor at the TU Delft. Although we could not meet face to face, Dr. Iulian Apachitei was able to skype with me and helped me through my thesis. He provided feedback on my work and research methods. His feedback has helped me to develop my research and professional writing skills further.
Furthermore, I wish to thank Dr. Amiq Gazdhar for giving me the opportunity to work in his biological laboratory and use his equipment. Without these resources, I would not have been able to complete this thesis research project. He was available for any questions and showed genuine interest in my work.
Last but not least, I would like to thank Danaël Gasser, for helping me solve practical problems and for the construction of the rotary device. Despite his busy schedule, he made time for me when I had questions.

Contents

Nomenclature

Roman Letters

Symbol	Description	Unit
E	Young's Modulus	[Mpa]
dP_{mean}	Mean systolic transvalvular pressure gradient	[mmHg]
Q	Flow rate	[mL/min]
Q_{RMS}	Root Mean Square value of systolic flow	[cm^3/s]
R	Resistance	[mmHg· min/mL]

Greek Letters

Symbol	Description	Unit
ΔP	Pressure gradient	[mmHg]
ε	strain	

Abbreviations

AV	AtrioVentricular
AX	Acetobacter Xylinus
BC	Bacterial Cellulose
DMSO	DyMethyl SulphOxide
ECM	Extra Cellular Matrix
EDV	End Diastolic Volume
EOA	Effective Orifice Area
ESV	End Systolic Volume
FDA	Food and Drug Administration
GAG	GlycosAminoGlycans
GOA	Geometric Orifice Area
PIV	Particle Image Velocimetry
PLA	PolyLacticAcid
RDR	Rotating Disc Reactor
SAVR	Surgical Aortic Valve Replacement
SEM	Scanning Electron Microscopy

SL	Semi-Lunar
SV	Stroke Volume
SVR	Surgical Valve Replacement
TAVR	Trans-catheter Aortic Valve Replacement (also termed TAVI; TAV-Implantation)
TEHV	Tissue Engineered Heart Valve
TVR	Trans-catheter Valve Replacement

Introduction

As the population ages and the know-how of the medical field progresses, the number of surgical interventions is rapidly expanding. Heart valve replacement surgery is no exception to this phenomenon; every year 280 000 heart valve replacement surgeries are performed worldwide [50]. Despite the success of heart valve replacement surgeries, various notable drawbacks hinder its advancement. Mechanical heart valves require anticoagulant therapy to reduce the risk of thromboembolisms, thereby also introducing anticoagulant-induced haemorrhage [20]. Furthermore, the need for anticoagulant therapy makes the mechanical valve undesirable for woman who desire a pregnancy. Bioprosthetic heart valves suffer from structural valve deterioration and therefore need to be replaced after less than 15 years [51][Figure I.1]. Replacement surgery is dangerous, with an increased mortality rate of up to 20% [63]. Furthermore, heart valve prosthetics do not allow for native cell tissue ingrowth, limiting their ability to self-repair and grow, the latter being of especially high importance in pediatric heart valve surgeries.

A promising new concept is the tissue engineered prosthetic heart valve, which would hypothetically remove the need for anticoagulent use, allow for self-repair and growth and increase the durability of heart valve prosthetics [51],[42],[53]. The process of creating a Tissue Engineered Heart Valve (TEHV) is, however, complex, and an optimal scaffold is yet to be found [43].

Fig. I.1: *A deteriorated bioprosthetic heart valve [16]*

Bacterial Cellulose (BC) is hypothesised to be a feasible scaffold and material for use in heart valve prostheses. BC is a biogenic polymer with a chemical structure not unlike collagen. The material is produced by, among others, the bacterium *Acetobacter Xylinus*. BC has been shown to have considerable mechanical strength and low thrombogenicity [68]. Furthermore, a study in rat models has indicated no inflammatory or foreign body response to implanted cellulose [30]. Bacterial cellulose is already successfully in use as wound dressing [11], and has been utilised to produce feasible vascular grafts [68], [3]. However, to the knowledge of the author, pure BC has not yet been used for the production of prosthetic heart valves.

The goal of this master thesis was to create the BC in a static and dynamic fashion. The BC was characterised by inflation testing, with the aim to create biogenic polymer heart valves, which would be tested in a pulsatile flow-loop.

Chapter 1

Technical Background

1.1 The Native Aortic Valve

The understanding of the native heart valve anatomy and characteristics is essential for the design of a prosthetic heart valve. The focus of this chapter is on the aortic heart valve, since this valve is most frequently diseased [53]. Furthermore, the test set-up used to test the valves produced during the master thesis research is designed to test aortic heart valves.

This section will discuss the anatomy and physiology of the heart, macro and micro-anatomy of the aortic heart valve and valve mechanical characteristics.

1.1.1 Anatomy and Physiology of the Heart

The human heart is separated into two sections, which both consist out of an atrium and a ventricle. Blood enters the heart via the atria, which fill until their pressure exceeds the pressure in the ventricles. The atrioventricular valve opens, and blood flows from the atria into the ventricles. The ventricles contract shortly afterwards, forcing the blood into the outflowing arteries. The right section of the heart circulates blood through the pulmonary circulation, while the left section pumps blood into the systemic circulation. While the pulmonary circulation is a small, low-pressure, system of blood vessels leading blood through the lungs, the systemic circuit is the large system of blood vessels running through all other parts of the body. Two heart valves, the *atrioventricular (AV) valves*, connect the atria to the ventricles. The two *semilunar (SL) valves*, named so because of their semilunar attachment shape [31], connect the ventricles to the outflowing arteries. The heart valves ensure unidirectional blood-flow. The tricuspid valve connects the right atrium to the right ventricle, while the pulmonary valve connects the right ventricle to the pulmonary artery. The left atria is connected to the left ventricle via the mitral valve, while the left ventricle is connected to the aorta via the aortic valve. While the SL valves and the tricuspid valve consists out of three leaflets, the bicuspid mitral valve only has two leaflets (two 'cusps'). Figure 1.1a shows a top view of the heart, where the four valves with their different leaflet morphologies can be distinguished.

Figure 1.1b shows the basic anatomy of the aortic heart valve. The location of the basal heart valve leaflet attachment, is called the *annulus*. The aorta bulges slightly above the aortic heart valve leaflets, forming the so-called sinuses of Valsalva. The location where the sinuses of Valsalva end, is named the *sinotubular junction* [31]. The location where the leaflet connection to the aortic wall reaches the sinotubular junction, is termed the *commissure* [39]. When

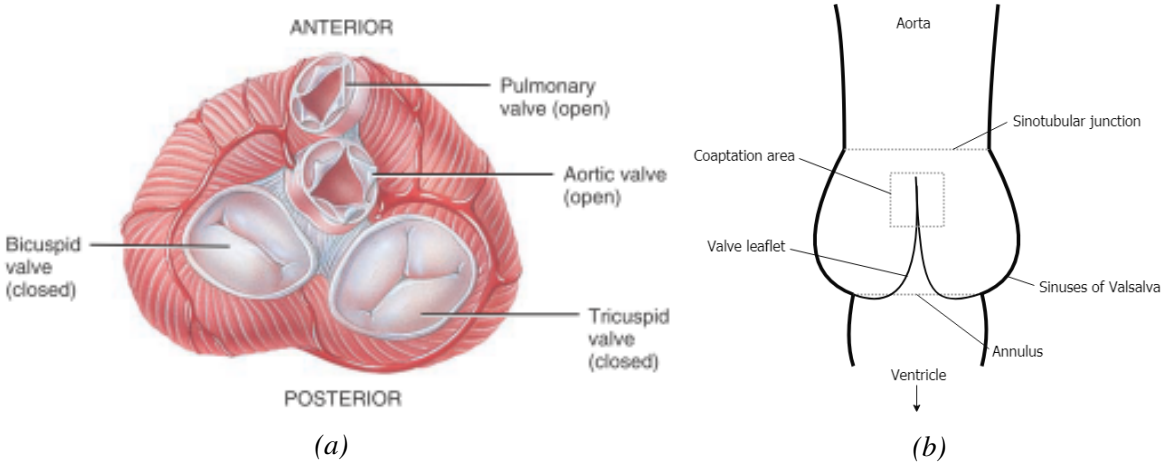

Fig. 1.1: *(a) Anatomy of the human heart seen from above [41] and (b) anatomy of the aortic heart valve*

the valve is closed, the three leaflets touch at the tips and overlap. This contact area is called the *coaptation area*. The leaflet overlap ensures no blood flows back through the valve during ventricular systole.

The systemic circulation is larger than the pulmonary circulation, leading to higher pressures and a higher flow resistance in the left heart section. The aortic valve therefore needs to withstand the highest pressures out of all valves.

The mechanical cycle of compression and relaxation of the heart chambers can be observed in Figure 1.2. The relaxation phase is known as the diastolic phase, while the contraction phase is named the systolic phase. Figure 1.2 starts during the resting phase of the heart; blood fills the atria. The atrial pressure exceeds the ventricular pressure, forcing the AV-valves open. A last atrial contraction forces the last blood into the ventricles. Shortly after, the ventricular systole starts. The ventricles contract and push blood into the arteries. The SL-valves open, again due to the pressure gradient between the ventricles and arteries, while the AV-valves close. While the SL-valves are open, the arterial and ventricular pressure are approximately equalised.

In a healthy adult, the aortic valve opens when a pressure of around 80 mmHg is reached. This pressure is termed the *diastolic aortic pressure*. The pressure during the ejection phase normally reaches about 120 mmHg. This pressure is termed the systolic aortic pressure. At the end of the ventricular systolic phase, the ventricles relax, causing the ventricular blood pressure to drop.

1.2 State Of The Art Prosthetic Heart Valves

The two main types of currently used prosthetic heart valves are mechanical heart valves and bioprosthetic heart valves. Bioprosthetic heart valves can be divided into Surgical Valve Replacements (SVR), Trans-catheter Valve Replacements (TVR) and Tissue Engineered Heart Valves (TEHV). Figure 1.3 shows examples of the main four prosthetic valves. TEHV are however not yet available on the market.

The most frequently used mechanical heart valve is the bileaflet valve, shown in Figure 1.3. Mechanical heart valves are the most durable heart valves currently on the market (20-30

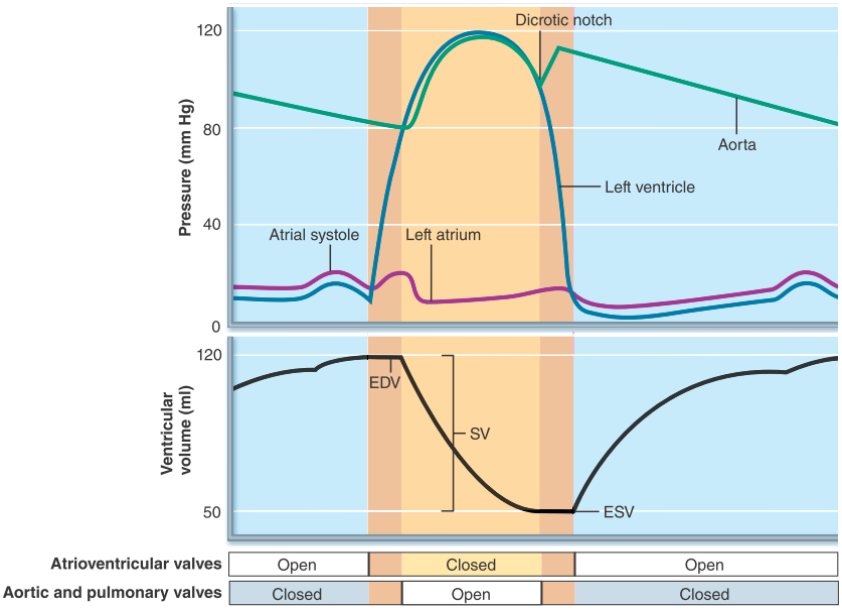

Fig. 1.2: *Pressure and volume changes during the cardiac cycle of the left atrium and ventricle [41]. The yellow phase and initial orange phase indicate the ventricular systole, while the blue phase and second orange phase indicate the ventricular diastole. EDV = End Diastolic Volume, SV = Stroke Volume, ESV = End Systolic Volume.*

years)[62]. A durable valve removes the need for re-operations in younger patients, reducing the associated infection and complications risk. However, due to the risk of thromboembolism (thrombus = blood clot, embolism = vessel blockage by loosening of clot), mechanical valves require life long anticoagulation therapy. Furthermore, this anticoagulant therapy itself can induce hemorrhage (excessive bleeding) [20]. These risks increase with age, making the mechanical valve less favorable for patients above 60 years old [62].

Bioprosthetic valves are constructed out of fixated biological tissues. Either a complete valve is harvested together with a section of the aorta, or the tissue is molded into three leaflets and sutured onto a metallic stent. They can either be surgically implanted (SAVR) or implanted using a catheter.

Bioprosthetic valves are virtually non-thrombogenic, eradicating the need for anticoagulation therapy. However, their low durability (10-15 years) makes them unattractive for younger patients [62]. Bioprosthetic valves are therefore mainly used for patients above 60 years old. The reason for low durability of bioprosthetic valves is still vague, although it is hypothesised to originate from, among others, valve leaflet calcification [62].

Tissue Engineered Heart Valves, TEHVs, provide a promising alternative for existing heart valve prostheses, since they promise i.e. complete biocompatibility and valvular regeneration, growth and repair.

TEHVs can be produced in three ways: *in vitro, in vivo* and *in situ* [23]. *In vitro* TEHVs are produced by seeding a scaffold with autologous cells and allowing for growth in a bioreactor. *In vivo* TEHVS are created by implanting a scaffold into a human body and letting a fibrous capsule form around the non-degradable scaffold [29]. In situ TEHVs are scaffolds implanted into the human body which are designed to recruit endogeneous cells. The scaffold needs to function as a heart valve until cells have grown into the scaffold, forming a new heart valve.

Current TEHVs are not feasible yet, since their polymeric scaffolds are not able to outper-

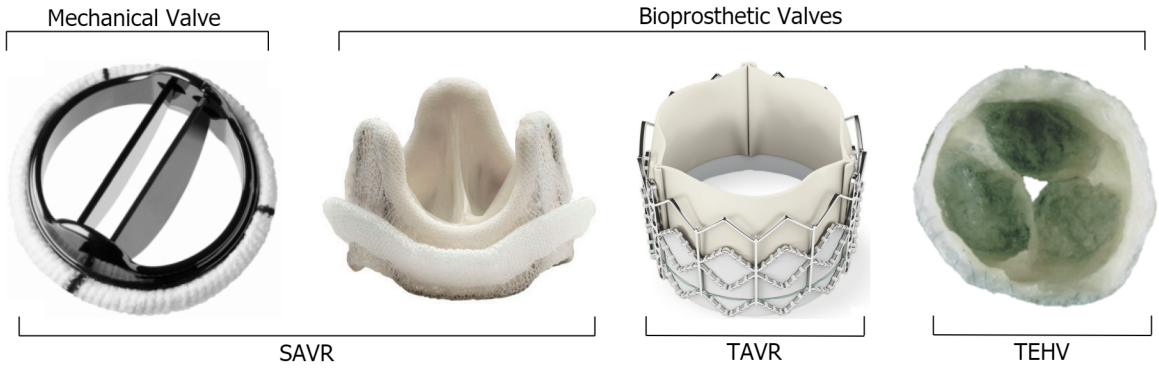

Fig. 1.3: *Types of aortic valve replacements. From left to right: SJM Regent (St. Jude Medical), Carpentier-Edwards (Edwars Lifescience Corp.), Sapien XT (Edwards Lifescience Corp.), tissue engineered heart valve [32]. SAVR: Surgical Aortic Valve Replacement, TAVR: Trans-catheter Aortic Valve Replacement, TEHV: Tissue Engineered Heart Valve. Figure adjusted from [27].*

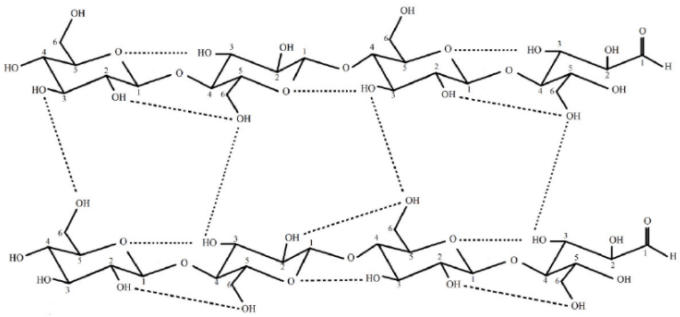

Fig. 1.4: *Chemical microstructure of BC fibrils [18]*

form natural tissues and bioprosthesis [23].

1.3 Bacterial Cellulose

Bacterial cellulose (BC) is a biogenic polymer produced by bacteria. The material consists out of fibrils constructed from glucose monomers [18], [Figure 1.4]. The molecular formula for one BC monomer is $(C_6H_{10}O_5)_n$. Several cellulose fibrils (ø2-4 nm) bond together by means of hydrogen bonds to form protofibrils. Protofibrils combine together to form nanofibrils (ø100 nm). The nanofibrils make up the fibrous network of BC. Figure 1.4 shows two separate fibrils of BC connected by hydrogen bonds. Due to its fibrilous structure, BC is often compared to extra-cellular matrix (ECM) components like collagen [19], [22], [48].

BC has a highly porous structure and good water holding capacity. It therefore acts similar to a hydrogel [19]. For different uses BC can be dried, but this process cannot be perfectly reversed. After drying, the water holding capacity of BC is greatly reduced [22].

1.3.1 Biocompatibility

The polysacharide chains of BC are not well recognisable by the human immune system, rendering the BC fibrils immunologically nonreactive [48]. Due to the absence of cellulose-

digesting enzymes in the human body, BC biodegradability is minimal [30]. The presence of endotoxins (i.e. bacterial residues) in biogenic polymers is to be considered before implantation. The endotoxin levels in BC has been determined to be lower than the set limit by the FDA (Food and Drug Administration). Namely, Bodin et al. [5] found an endotoxin concentration of 0.1 endotoxin units (EU)/ml, while the FDA limit is at 0.5 (EU)/ml.

BC has been implanted in rat models by Helenius et al. [30] and in mice by Mendes et al. [44]. Helenius et al. observed no foreign body response and found blood vessels growing into the cellulose tissue. Mendes et al. also found no evidence of an inflammatory reaction after 90 days of implantation. Implantation of BC tubes as vessel substitutes by Schumann et al. again showed no evidence of inflammation [55].

Cellular ingrowth into BC is found to be possible by several authors, while this is contradicted by others. Mendes et al. concluded that implanted BC parts where encapsulated by fibroblasts and collagen fibers, but fibroblasts did not penetrate into the BC, because of a too small pore size. Schumann et al. and klemm et al. found fibroblasts growing into the BC tissue [55], [36]. Backdahl et al. seeded BC samples with smooth muscle cells, and observed the cells attaching to the BC and pushing cellulose fibers away in order to migrate into the material [2]. Human chondrocytes were also found to migrate into BC material after seeding [59].

1.3.2 Mechanical Properties

Mechanical properties of BC have been reported with great variance. The Young's Modulus of BC has been reported to be between 0.6-2700 MPa, while the tensile strength of the BC has been reported to lie around 0.16-300 MPa [2][37][59][7][67]. For a more detailed overview, the reader is referred to the literature study preceding this work [57].

1.3.3 Applications

Several BC material applications have been approved by the FDA: MTA^{TM} Surgical Sheet and Securian^{TM} Tissue Reinforcement Matrix are FDA approved medical devices made out of BC. Furthermore, Xylos Corporation® sells Xylos® Surgical Mesh, Xylos® Vessel Guard and Xylos® Porous Surgical Mesh. BC is mainly used in the medical field as wound dressing [11]. Other applications include dura mater prostheses, nerve surgery covers, artificial skin [49] and arterial stent coating [12]. [48]. BC tubes have been successfully used as blood vessel replacement by multiple other authors, including Schumann et al. [55], Klemm et al. [36], Wurdinger et al. [66], Wipperman et al. [65] and Zahedmanesh et al. [68].

A further investigated application of BC is the use as a bone tissue scaffold. Hutmacher et al [33] and Fang et al. [21] have used a hydroxyapatite-BC composite seeded stem cells from human bone marrow as bone construct. Their results showed cell differentiation, attachment and proliferation. This process however still needs optimization and further investigation into the alterations of the hydroxyapatite-BC scaffold characteristics.

BC is additionally investigated as a artificial cornea or cornea scaffold for eye tissue engineering [25], [15].

1.4 Technical Background

To describe and analyze the performance of a prosthetic valve, several definitions are of importance. The terms discussed below are all related to the SL-valves, since the experimental setup used during the project is designed to test these valves. As mentioned before, special attention is payed to the aortic heart valve.

1.4.1 Transvalvular Pressure Gradient

The transvalvular pressure gradient indicates how well the valve is opening during systole. Ideally, the blood can flow unobstructed from the ventricle to the aorta, in which case the pressure gradient would be equal to zero. Under laminar flow conditions, the pressure gradient can be described by Equation 1.1 [Klabunde].

$$\Delta P = Q \cdot R \tag{1.1}$$

Here Q is the flow rate, and R the resistance. As discussed before, a stenotic valve has a significantly higher pressure gradient due to the increased resistance caused by insufficient valve opening. A higher pressure gradient therefore indicates a lesser valve performance.

1.4.2 Effective Orifice Area

The opening area of the heart valve is termed the geometric orifice area. The geometric orifice area, GOA, is not a good indicator of how well the valve allows for unobstructed blood flow. Namely, after flowing through the valve, the flow jet contracts slightly before expanding, forming the *Vena contracta* [14]. This contraction is caused by the abrupt narrowing of the flow path (from ventricle to aorta) [1]. A more abrupt narrowing results in a continued acceleration of the flow jet after it has passed through the opening. This continued acceleration causes the flow jet to contract just after the valve opening. At the point of maximum contraction, a new orifice area can be measured; the Effective Orifice Area (EOA).
This measure is a widely used prosthetic valve characteristic to determine valve efficiency. The EOA indicates the effective valve opening during systolic blood flow through the valve [14]. It can be computed using the Gorlin relation, see Equation 1.2 [54].

$$EOA = \frac{Q_{\mathrm{RMS}}}{51.6 \cdot \sqrt{dP_{\mathrm{mean}}}} [cm^2] \tag{1.2}$$

Here Q_{RMS} [cm^3/s] is the Root Mean Square value of the systolic flow through the valve and dP_{mean} [mmHg] the mean systolic transvalvular pressure gradient.
From Equation 1.2 it is clear that the effective orifice area will increase if the flow through the valve increases and the pressure gradient decreases. To accomplish this, the valvular resistance has to decrease, see Equation 1.1. The EOA is effectively a measure of the resistance of the valve to unobstructed blood flow. A higher effective orifice area is therefore beneficial for valve performance.

In general, mechanical valves, stentless valves and newer model valves have a larger EOA [50]. Naturally, valves with larger GOA's will have larger EOA's. One should therefore only compare valves of the same size to determine which valve has larger effective opening. To be able to compare EOA's of differently sized valves, the EOA is indexed by dividing it by the surface area of the valve (πr^2).

Chapter 2

Materials and Methods

2.1 Bacteria Handling

The bacteria used in this study were of the strain *Gluconacetobacter Xylinus* (ATCC®700178), acquired by the production firm ATCC: The Global Biosource Center (LGC Standards GmbH - Germany Office, 46485 Wesel, Germany).

Bacteria were stored in microcentrifuge tubes (2 ml) in 20% glycerol solution at -80 °C [8]. Agar plates for bacteria propagation were prepared using a recipe prescribed by the ATCC, see Appendix A. After autoclaving the agar, it was left at room temperature to cool down to approximately 40 °C, while shaking the bottle intermittently. The sterile agar was poured into a sterile Petri dish, after which it was allowed to harden at room temperature. One microcentrifuge tube was taken from the -80 °C fridge, thawed and spread on the agar. The dish was then closed and cultured in a bioreactor at 26 °C for 48 hours. Resulting colonies should be small, slightly irregular, smooth, entire, pulvinate and opaque according to the ATCC. Figure 2.1(a) shows the results of bacteria culturing after 72 hours of incubation.

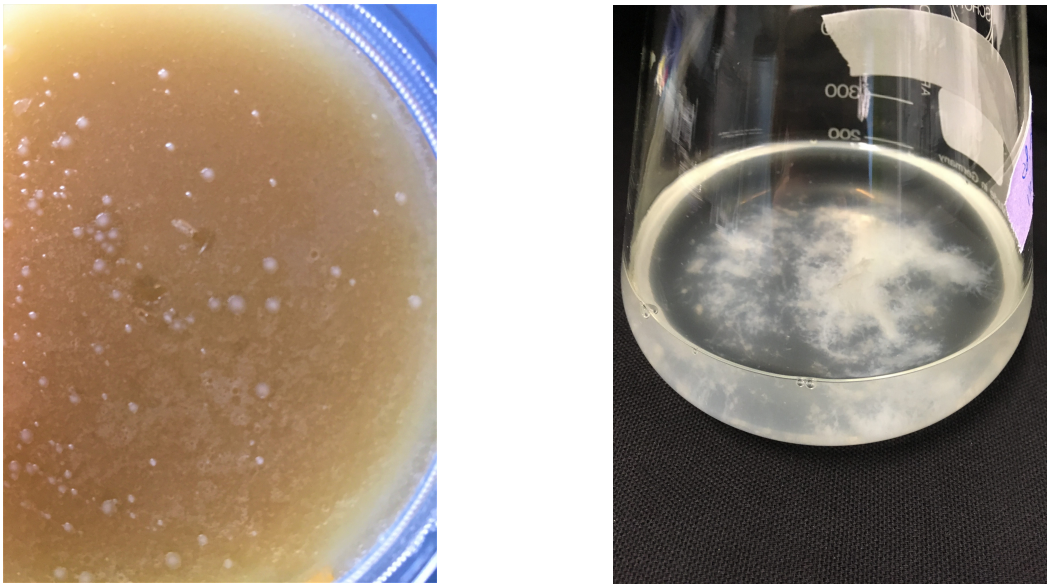

(a) Bacterial colonies on agar *(b) Bacterial inoculum*

Fig. 2.1: *(a) Agar plate after 72 hours of incubation. The small white dots on the surface represent bacterial colonies and (b) Inoculum after 48 hours of shaking at 240 RPM*

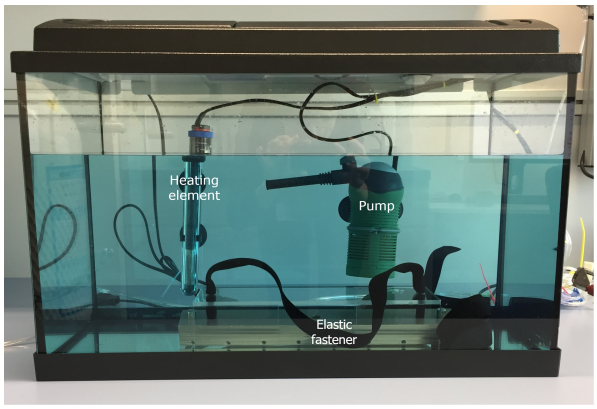

(a) Waterbath bioreactor

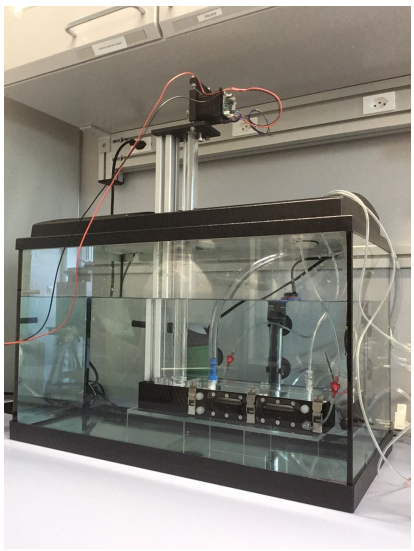

(b) Rotary device in the waterbath

Fig. 2.2: *(a) Waterbath for constant temperature maintenance. The blue hue originates from the anti-microbial sodium nitrit. The rubber band attached to the metal bar keeps down the incubation box for static culturing. (b) The waterbath for rotary culturing. The water is not blue; sodium nitrit has been removed to avoid damaging the rotary device.*

To increase the bacteria, 3-4 colonies were harvested with a pipette tip and transferred to 200 ml of glucose medium. This glucose medium was produced using a recipe found in Appendix A. This glucose medium is used in a patent by Winkler et al. [64]. The mixture of glucose medium and bacteria colonies was shaken in a shaker at 240 rpm for 48 hours. Figure 2.1(b) shows the resulting bacteria broth, now termed inoculum. New microcentrifuge tubes were filled with 700 μl of 20% glycerol solution and 700 μl of inoculum. Afterwards, the tubes were transferred to the -80 °C fridge for long-term storage. Every new BC production cycle, new bacteria were harvested by thawing a microcentrifuge tube from the -80 °C fridge and propagating it in the shaker using the method described above.

2.2 BC Production

2.2.1 Culturing Environment

A constant culturing environment was maintained by immersing the BC production casing within an in-house produced bioreactor [46]. The bioreactor consisted out of an aquarium filled with distilled water mixed with Sodium Nitrit to prevent microbial growth . An heat element in combination with a filtration pump ensured a constant temperature of 29°C inside the bioreactor. The aquarium was wrapped in isolation material to ensure minimal heat loss. The BC production casing was different for static and rotary culturing. For static culturing, a plastic incubation box was fastened to a stainless steel bar with a rubber band [Figure 2.2a]. During rotary culturing, the rotatary device was placed within the water bath [Figure 2.2b].

In static culturing, oxygenated gas is led through a gas supply tube to ensure a constant oxygen level inside the incubation box. To prevent drying of the BC within the incubation box, the gas supply tube is led through a miniature water bath. Inflowing gas is thereby hydrated be-

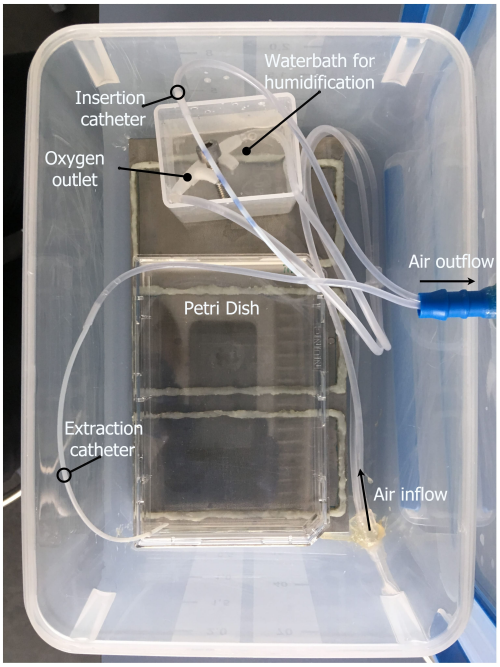

(a) Plastic incubation box. This image shows a Petri dish with lid-mounted catheters

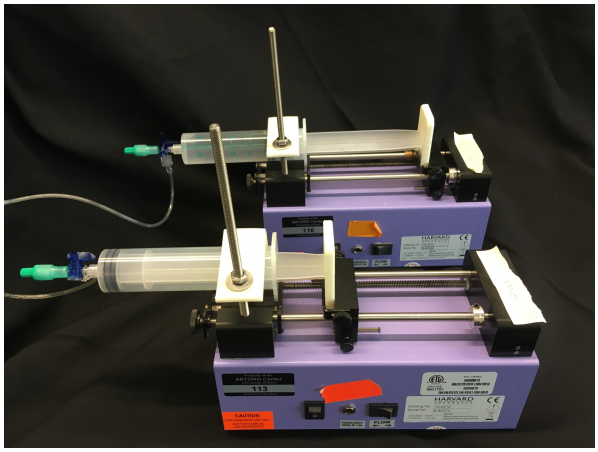

(b) Injection and extraction pump systems

Fig. 2.3: *(a) The plastic incubation box contains the Petri dishes and a small waterbath for air hydration. Oxygenated air is introduced into the box via a catheter, while waste gas can flow out through a tube in the lid. (b) The two pumps used for extraction and injection, with 50 mL syringes.*

fore entering. The oxygenated gas is a mixture of pure medical grade oxygen with pressurised air (78% N_2, 21% O_2, 0.9% noble gases, 0.04% CO_2, 0.00005% H_2). Both gases are mixed by use of a Y-trace tube splitter. The gases are led into the Y-trace splitter at a pressure of 1 bar. The oxygenated air within the incubation box therefore has a concentration of:

$$\%O_2 = 0.5 \cdot 21 + 0.5 \cdot 100 = 60\% \tag{2.1}$$

2.2.2 Stationary Culturing

For control and mechanical characterisation, BC was cultured in a stationary manner. Sterile Petri dishes (86mm by 128mm, Thermo Fisher Scientific, United States) were placed inside a plastic incubation box, which was submerged within the aquarium. A stainless steel plate is placed inside the plastic incubation box to further ensure that the incubation box remains submerged. Figure 2.3a shows the incubation box with its gas supply tube.

60 mL of the glucose medium was introduced into each Petri dish, after which 6 mL of bacterial inoculum resulting from bacteria propagation was added.

To produce BC, the Petri dishes were kept inside the bioreactor for 12 days. To ensure a constant medium exchange during culturing, sterilised in- and outflow catheters were connected to the Petri dishes using two different methods. As can be seen in Figure 2.4, catheters were either introduced into the medium through the lid, or through the walls of the Petri dish. Catheters were sterilised by flushing with 70% ethanol solution [9]. It is hypothesised that wall-mounted catheters do not perturb the cellulose growth, resulting in a more homogeneous patch.

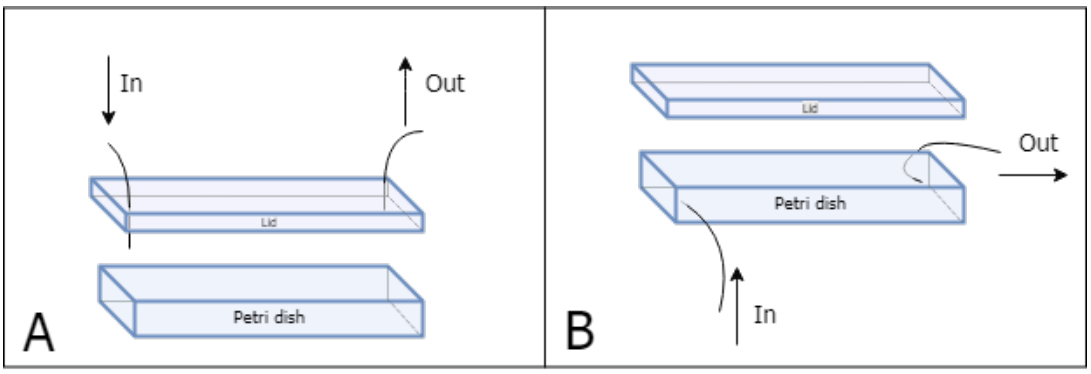

Fig. 2.4: *(A) Schematic drawing of the lid-mounted catheters, and (B) a schematic drawing of wall-mounted catheters*

However, contrary to the lid-mounted catheters, the wall-mounted catheter entrance holes have to be sealed with glue (Loctite Hysol M-31CL Medical Device Epoxy Adhesive, Henkel AG & Company, Düsseldorf, Germany), which could negatively affect the BC growth.

The catheters were connected to syringe pumps (Model 11 plus, Harvard Apparatus, Holliston, USA), which inject and extract medium at certain time intervals [Figure 2.3b]. The syringe pumps are controlled with MATLAB (MathWorks, Natick, MA, USA). 3D-printed adapters were introduced to allow for larger syringes to be used in the syringe pumps.

A pilot study with tap water and contrast fluid was performed into diffusion behaviour, in order to establish the best catheter configuration and injection speed. Tests were thereafter conducted inside the bioreactor with medium and BC producing bacteria.

2.2.2.1 Automatic exchange pilot study

A Petri dish identical to the one used for bacterial culturing was filled with 60 ml of tap water. Injection fluid was prepared using a mixture of tap water and the blue food colouring (E133, Cake iD BV, The Netherlands) with a concentration of 1:10. 1 ml of fluid is injected every 1440 seconds with a 30 ml sterile syringe (CODAN, Adelaide, Australia). The injection speed is varied per test. In this way, one test would take 12 hours and could be started in the evening and stopped in the morning. Tests were conducted at room temperature. Pictures were taken using a piA640-210gc GigE camera (Basler AG, Ahrensburg, Germany).

Figure 2.5(a) and 2.5(b) give a depiction of the different catheter mount methods used. Table 2.1 shows the four different tests that were conducted:

Tab. 2.1: *Pilot study tests of the diffusion rate in square Petri dishes*

Test	Injection speed [ml/min]	Extraction speed [ml/min]	Catheter mount method
Diffusion Test 1	1	1	Wall-mounted, Single inlet-outlet
Diffusion Test 2	2	1	Wall-mounted, Single inlet-outlet
Diffusion Test 3	1	1	Wall-mounted, Double inlet-outlet
Diffusion Test 4	3	3	Top-mounted, Single inlet-outlet

It is hypothesised that a faster injection speed will improve diffusion. Furthermore, a dual infusion/extraction system using four catheters is hypothesised to further improve diffusion. Lid-mounted catheters have been tested in case wall-mounted catheters would pose a problem to the growing cellulose.

The four catheter test was conducted using two infusion pumps, each connected to two catheters by means of luer connections. Injection and extraction is performed in a cross-wise fashion to ensure optimal diffusion.

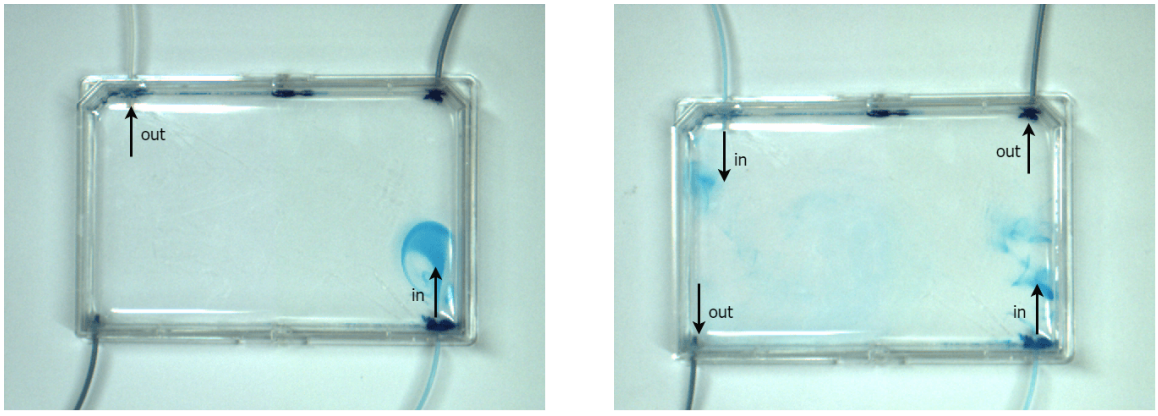

(a) Mono-injection system *(b) Dual-injections system*

Fig. 2.5: *(a) Injection and extraction using two catheters. Opposite corners are used to optimise diffusion throughout the dish. (b) Two catheters in opposite corners inject, while two others in opposite corners extract. This dual injection system is hypothesised to result in optimal diffusion.*

2.2.2.2 Automatic exchange in BC culturing

The different automatic exchange protocols were also tested with bacteria in the bioreactor. The injection volume was set at 0.5 mL, injected at a speed that varied per test. The waiting time is again set at to 1440 seconds, to ensure a full medium exchange every two days. Holes were drilled in sterile Petri dishes, in which catheters were inserted and glued depending on their position (no glue for lid-mounted catheters). The whole setup was thereafter sterilised

with 70% ethanol.

Petri dishes were filled with 60 ml of sterile glucose medium and 6 ml of inoculum. Injection and extraction of medium was started at the fourth day of culturing to give bacteria time to form a cellulose layer on top of the medium. Culturing was continued for a total of 12 days per test.

Table 2.2 shows the five different tests that were conducted in the bioreactor:

Tab. 2.2: *Bioreactor tests of the BC growth in square Petri dishes with different injection speeds*

Test	**Injection speed [ml/min]**	**Extraction speed [ml/min]**	**Exchange start day**	**Catheter mount method**
Exchange Test 1	2	1	4	Wall-mounted
Exchange Test 2	2	1	4	Top-mounted
Exchange Test 3	3	3	5	Top-mounted
Exchange Test 4	3	3	3	Top-mounted
Exchange Test 5	3	3	3	Top-mounted

The injection rates shown in Table 2.2 were based on the results of the pilot study into diffusion rates in square Petri dishes.

2.2.3 Rotary culturing

The study preceding this master thesis research [58] produced heart valves using BC produced in Petri dishes. This cellulose was sutured into a tube before it was sutured into a heart valve holder. The study results showed that the weakness of the produced BC heart valves was this particular suture line. Production of tubular BC is hypothesised to increase valve strength.

The production of tubular BC has already been achieved by Bodin et al. [3]. Namely, Bodin et al. submerged an oxygen permeable tube in medium and let it slowly rotate. BC would form on the surface of the tube; the location where oxygen and medium meet. In industry, tubular cellulose can be created using Rotary Disc Bioreactors. The method used for this master thesis research is based on both the method used by Bodin et al. and the method used in industry [28].

A rotary device was constructed by the workshop at the ARTORG Center. Detailed technical drawings can be found in Appendix C. A rotating stainless steel (Grade: X5CrNi18-10. Number: 1.4301) cylinder is placed within a rectangular box. The dimension of the cylinder allow for the production of tubular cellulose with an inner diameter of 22mm. The length of the cylinder allows for the creation of three heart valves out of one BC tube. A stepper motor (PD-1141, Trinamic Motion Control GmbH & Co. KG, Hamburg, Germany) drives the steel cylinder by a drive belt. In this way, the cylinder can be submerged in the aquarium for temperature control, while the motor can be situated above the aquarium. The motor is connected to a variable power source (DF-1730SB, Distrelec Group AG., Nänikon, Switzerland) and to a laptop with driver software (Trinamic IDE 3.0, Trinamic Motion Control GmbH & Co. KG, Hamburg, Germany). The driver software allows for control of the motor RPM. Figure 2.7 shows the rotary device and a close-up of the incubation box with the stainless steel cylinder.

The box has four luer connections that allow for medium exchange catheters to be connected in a water-tight manner. Oxygen can be led into the box with the cylinder via another luer

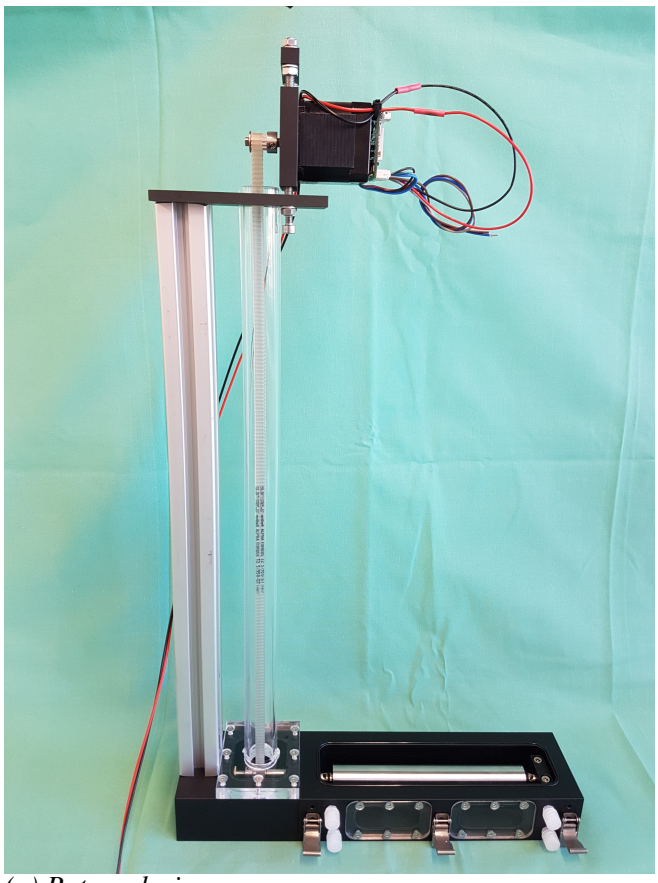

(a) Rotary device

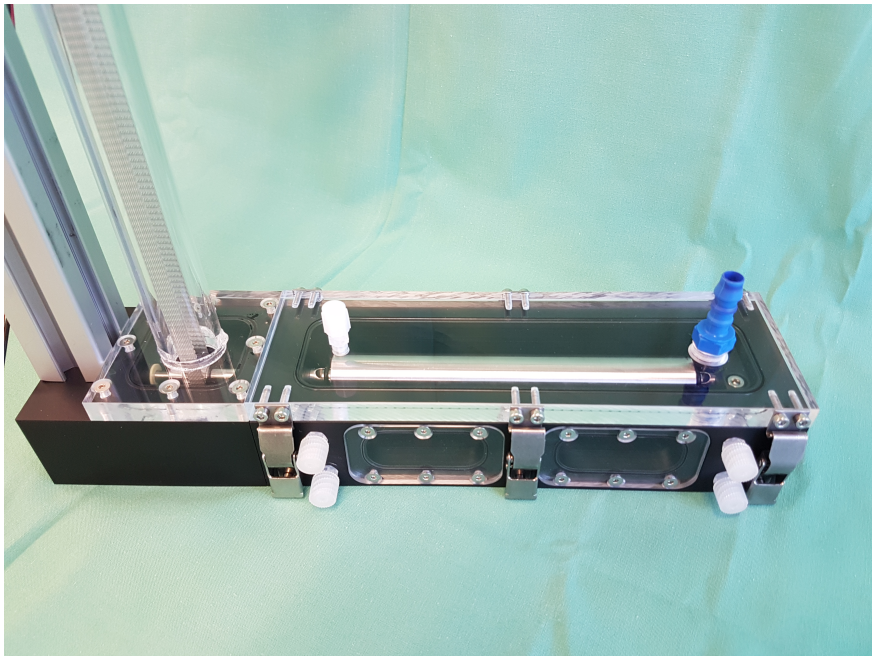

(b) BC containing incubation box of the rotary device

Fig. 2.6: *(a) The rotary device with top-mounted engine. The engine drives the stainless steel cylinder in the incubation box with a rubber drive belt. In this way, the incubation box can be submerged, while the engine is above the water level. (b) The incubation box of the rotary device. The stainless steel cylinder can be easily taken out after culturing. A Plexiglas lid and two Plexiglas windows allow for visual inspection during culturing. Luer connectors at the side allow for connection of catheters for medium exchange and oxygen inflow.*

connection, while waste gas is removed through a tube connected to the top of the box. Two Plexiglas windows and a Plexiglas lid allow for visual inspection during culturing.

Four pilot tests were conducted using the rotary device. All tests were conducted outside the aquarium, without addition of oxygen. These variables will be introduced after a feasible production method has been established. Test 1, 2 and 3 were run for 7 days. Test 4 was run for 11 days. Injection and extraction of medium was always started at the third to fifth day, to give the bacteria time to adhere to the surface. Injection and extraction was performed at a speed of 1 ml/min. Table 2.3 gives an overview of all different tests conducted:

Tab. 2.3: *Bioreactor tests of the BC growth in square Petri dishes with different injection speeds.*
[a] Silicon by: Sylgard 184 Silicone Elastomer, Dow Corning, Midland, Michigan, US.
[b] Silicon by: Maagtechnic AG, Füllinsdorf, Switzerland

Test	**Injection speed [ml/min]**	**Extraction speed [ml/min]**	**Interval time [s]**	**Rotation speed [rpm]**	**Material**
Rotary Test 1	1	1	2880	1	Stainless steel
Rotary Test 2	1	1	1440	0.2	Silicon coating[a]
Rotary Test 3	1	1	1440	0.2	Polyethylene, Polypropylene, Roughed stainless steel
Rotary Test 4	2	2	1440	0.5	Silicon tube[b]

Figure 2.7a shows the cylinder in the rotary device. Half of the cylinder was roughed by sanding. One eight was covered with a solid polyethylene ring. One eighth was covered with a solid polypropylene ring, while the last section was covered with polyethylene foil (kitchen foil). In Rotary Test 4, adapter parts were 3D printed (Polylactic Acid [PLA]) in order to connect the silicon tube to the rotary device. Figure 2.7b shows the silicon tube in the rotary device.

pH of the medium was mesured after culturing, using a pH meter (SevenEasy, Mettler-Toledo International inc., Columbus, Ohio, US).

2.2.4 Post-Processing of Cellulose

To remove and kill the bacteria, the matured cellulose patches were post-processed. The patches and BC resulting from rotary culturing were transferred to distilled water and boiled for 30 minutes at 80°C. Thereafter they were cooled down and transferred to a 0.3 molar sodium hydroxide (NaOH) solution, and again boiled at 80°C for 30 minutes. After cooling down, the patches were cleaned by gently shaking them in distilled water. They were finally stored in distilled water.

(a) Test 3 with four different material sections on the cylinder

(b) Test 4 with a silicon tube. Two adapters connect the tube to the rotary device

Fig. 2.7: *(a) The adapted stainless steel cylinder: the proximal section is roughened stainless steel, the black ring consists out of polypropylene, the white ring out of polyethylene. The distal section is covered in polyethylene foil (kitchen foil). (b) The silicon tube inside the rotary device.*

2.3 BC Characterisation

2.3.1 Density Determination

To qualitatively determine the density of the material, the fibrous structure of the BC was analysed using Scanning Electron Microscopy (SEM). Before imaging, BC samples were freeze-dried for one night (Mini Lyotrap, LTE Scientific Ltd, Greenfield, Oldham, Great Britain). They were subsequently gold coated (JFC-1300 Auto fine coater, Jeol Ltd, Akashima, Tokio, Japan), and imaged in a scanning electron microscope (JSM-IT100, Jeol Ltd, Akashima, Tokio, Japan).

2.3.2 Strain testing

Finished BC patches were inflated using a custom made inflation device [46], to test the mechanical and creep behaviour of the BC. Each patch is cut into two circular patches, one circular patch out of each half of a square BC patch. Each circular patch is termed after the Automatic Exchange test patch number from which they were cut, with the addition of 'A' or 'B'. Patch names therefore go from Test 1A, to Test 4B. A commercially available bovine pericardium patch (CARDIO CEL, Admedus Regen Pty Ltd, Malaga Western Australia, Australia) is tested as a reference. These pericardium tests were conducted by Andrea Nienhaus [46].

Figure 2.8 shows a schematic overview and an image of the inflation set-up. This device has been based on the designs presented by W. Buerzle et al. [6] and E. Chanliaud et al. [7]. The device has been constructed with the help of Prof. Dr. Edoardo Mazza, ETH Zürich [46]. Detailed drawings can be found in Appendix B.

The patch is inflated by connecting the basal side of the patch to a water column, while the water on the apical side of the patch is not in contact with said water column. Water on the apical side is needed to keep the patch from drying out. In this way, a pressure difference can be created, inflating the patch. Pressure is measured at the ground, on the basal side of the patch. Pressure is measured with disposable pressure sensors (PX600F 150B, Edwards Lifesciences, CA, USA). A high-speed camera (Basler piA640-210gc GigE, Basler AG, Ahrensburg, Germany) is mounted normal to the patch surface. Images are taken at a frequency of 1 Hz. The water column is slowly filled with water, raising the pressure to approximately 100 mmHg. After conducting a creep test, pressure is raised to 160 mmHg.

To visualise the strains on the patch surface, the method of Particle Image Velocimetry (PIV) is used. Particles are scattered on the patch surface. Images are taken at different time points. These images are filtered in order to improve particle visibility. Figure 2.9 shows the image after all filters have been applied. The image is cropped, converted to grayscale and noise reduced using a Gaussian filter. It is subsequently sharpened, inverted and a threshold is applied. Edges and particles surrounding the patch were masked.

A specialised PIV software[61][60] analyses the images by tracking the particles and computing the displacement. The displacement of the particles were converted into strains by use of the 2D Cauchy strain tensor, see Equation 2.2. This equation is valid for infinitesimal strains. The conversion was done in MATLAB (MathWorks, Natick, MA, USA).

ε_{xy} is considered equal to ε_{yx}, since the material is assumed to be homogeneous.

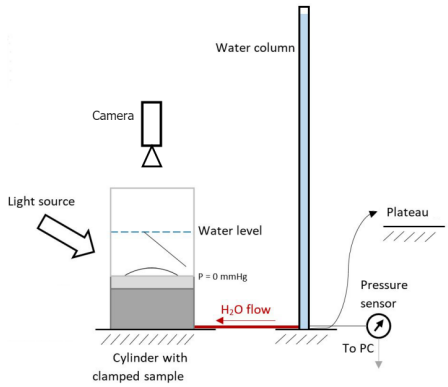

(a) Schematic overview of the inflation set-up. Taken from [46] and adjusted.

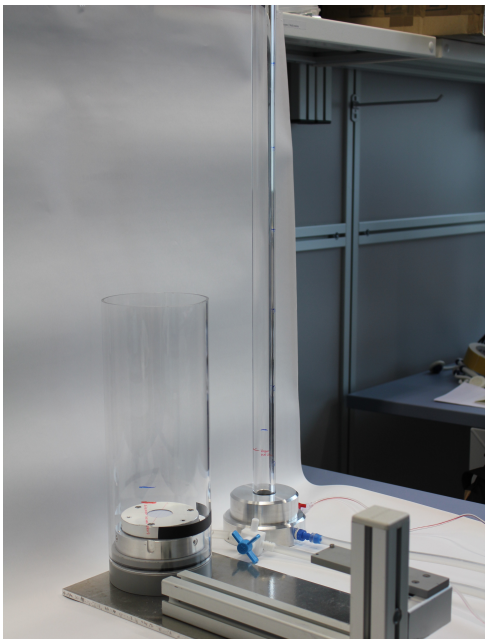

(b) The inflation set-up with the water cylinder and water column [46]

Fig. 2.8: *(a) Schematic overview showing how the basal end of the patch is connected to a water column. The apical side is submerged in order to keep the patch from drying out. The water column can be moved to higher standing plateaus to increase the pressure. (b) The set-up in real life.*

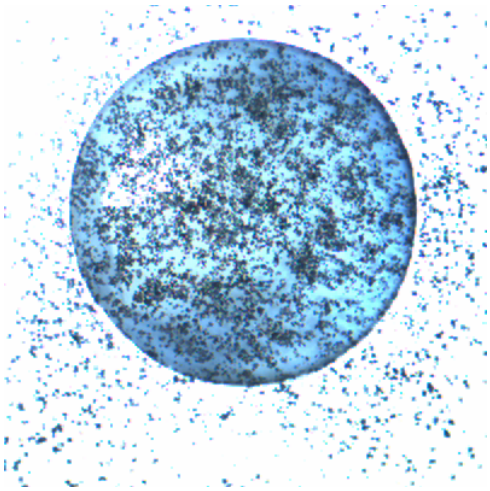

(a) Image taken by the camera during testing

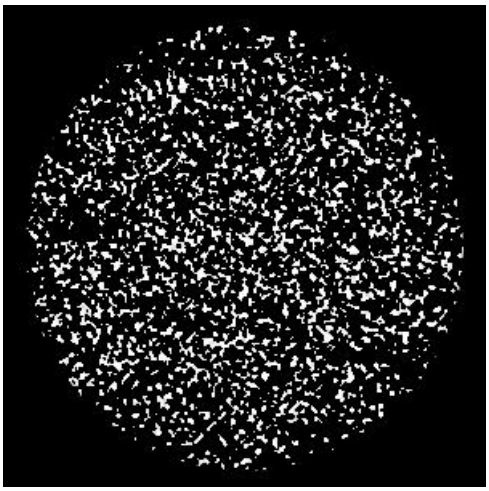

(b) Image after processing

Fig. 2.9: *(a) A captured image during inflation testing and (b) the same image after cropping, converting to grayscale, Gaussian filtering, sharpening, application of a threshold and removal of edges.*

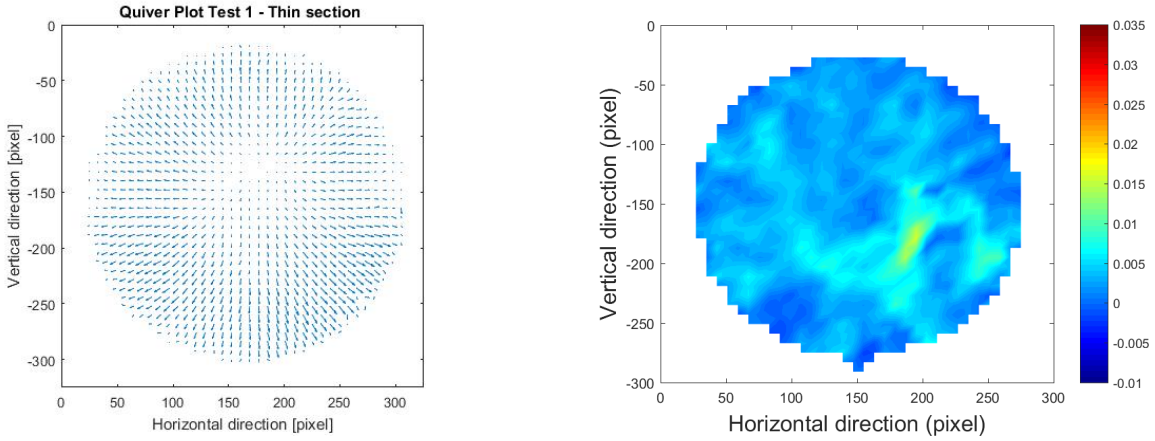

(a) Quiver plot *(b) Colour plot or strain map*

Fig. 2.10: *(a) Quiver plot showing the direction and magnitude of movement of pixels. (b) Colour plot showing the magnitude of principal strain at different locations of the patch.*

$$\varepsilon = \begin{bmatrix} \varepsilon_{xx} & \varepsilon_{xy} \\ \varepsilon_{yx} & \varepsilon_{yy} \end{bmatrix} = \begin{bmatrix} \frac{\delta u}{\delta x} & \frac{1}{2}\left(\frac{\delta u}{\delta y} + \frac{\delta v}{\delta x}\right) \\ \frac{1}{2}\left(\frac{\delta v}{\delta x} + \frac{\delta u}{\delta y}\right) & \frac{\delta v}{\delta y} \end{bmatrix} \tag{2.2}$$

The PIV software creates a matrix with a deflection for every pixel of the image. The deflections were visualised by constructing a quiver plot in MATLAB. Figure 2.10a shows an example of the quiver plot. The strain was visualised by a colour plot (Figure 2.10b) of the maximum principal strains. A colour plot was constructed using MATLAB. The principal strain was computed using Equation 2.3.

$$\varepsilon_{max} = \frac{\varepsilon_{xx} + \varepsilon_{yy}}{2} + \sqrt{\left(\frac{\varepsilon_{xx} - \varepsilon_{yy}}{2}\right)^2 + \left(\frac{\varepsilon_{xy}}{2}\right)^2} \tag{2.3}$$

A strain map is constructed separately for the pressure increase of 0 to 100 mmHg, and for the pressure increase of 100 mmHg to 160 mmHg. The strain maps of the higher pressure levels therefore show the strain relative to the end position of the patch at 100 mmHg.

To construct pressure-strain and creep graphs, the average principal strain was computed for different stages of patch deflection. The average principal strain was computed over the middle section of the patch [Figure 2.11]. This averaging was applied to minimise erroneous strains on the edges due to out-of-plane movement. The circle is defined by a diameter half the diameter of the patch.

Creep tests are conducted for 20 minutes at 100 mmHg, and for 20 minutes at 160 mmHg. The inflation device is not completely tight due to the inhomogeneity of the BC patch. This inhomogeneity causes improper clamping. Therefore, under higher pressures, water slowly flows from the water column, through the clamping structure, to the water reservoier at the apical side of the patch. During creep testing, this leakage prevents a constant pressure during 20 minutes of testing. An infusion dripping bag is used to slowly drip water into the water column. The inflowing water corrects for the water leaving the water column through due to the leakage. At the same time, water is kept at a constant level in the water reservoir at the apical side of the patch, by letting water flow out through a luer opening.

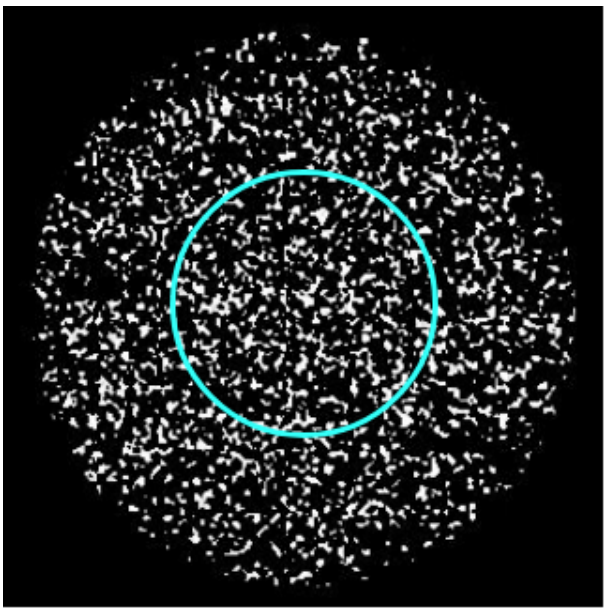

Fig. 2.11: *Section used for principal strain averaging*

Chapter 3

Results

The following chapter describes the results of all conducted tests. These include the results of stationary culturing, rotary culturing and BC characterisation.

3.1 Stationary Culturing

3.1.1 Pilot Study Automatic Medium Exchange

Figure 3.1 shows the results of Diffusion Test 1, testing with an injection speed of 1 ml/min. The diffusion rate is relatively fast; contrast fluid is dispersed over the entire Petri dish after 3 hours. The contrast fluid has diffused homogeneously after 6 hours. Figure 3.2 shows the

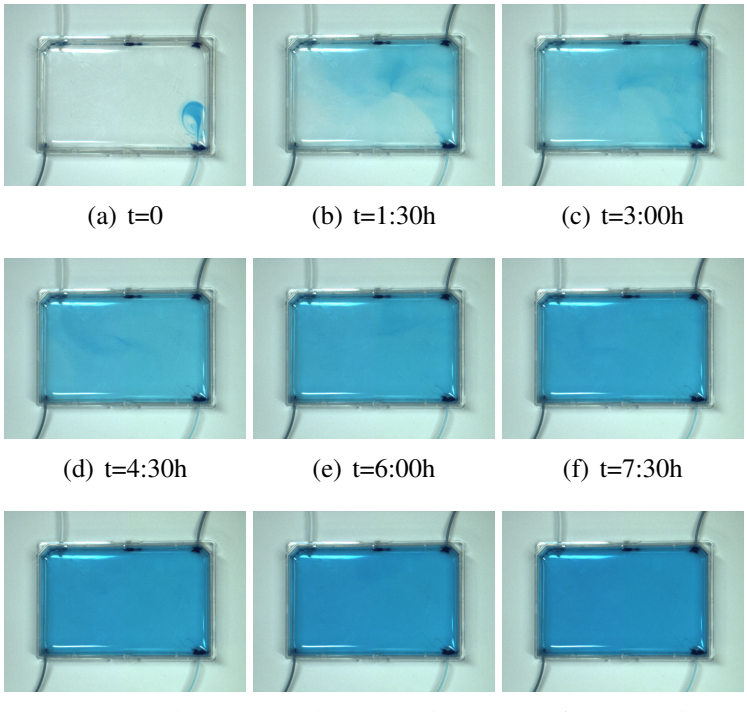

(a) t=0 (b) t=1:30h (c) t=3:00h

(d) t=4:30h (e) t=6:00h (f) t=7:30h

(g) t=9:00h (h) t=10:30h (i) t= 12:00h

Fig. 3.1: *Diffusion Test 1 in a Petri dish with a 1 ml/min injection speed as a function of time*

results of Diffusion Test 2; a setup with an injection speed of 2 ml/min. A faster injection speed

improves the diffusion rate, although not significantly. The contrast fluid fills the Petri dish after 3 hours, and is homogeneously diffused after 6 hours. The test differs from Test 1, in that the contrast fluid looks more dispersed after 3 hours, and more homogeneous after 6 hours. Figure

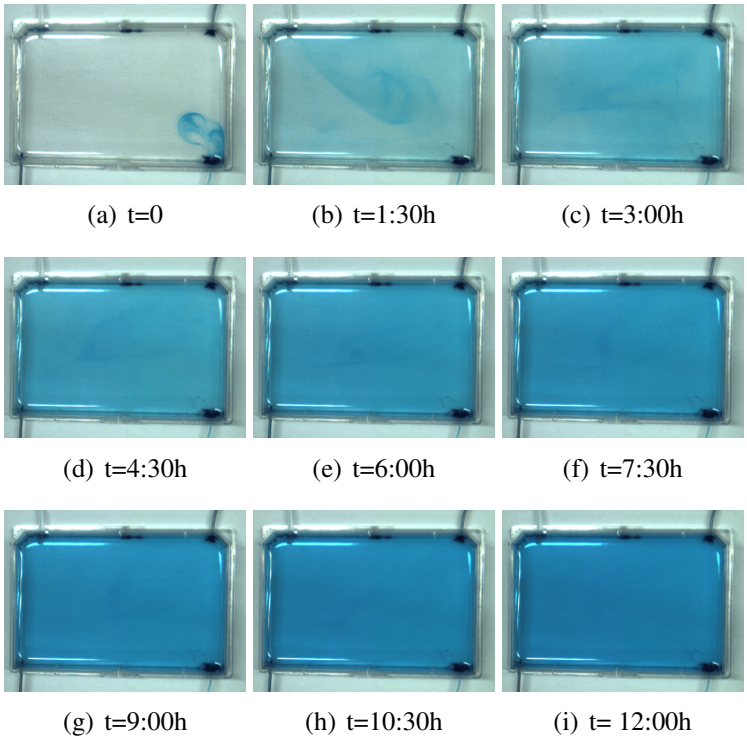

(a) t=0 (b) t=1:30h (c) t=3:00h

(d) t=4:30h (e) t=6:00h (f) t=7:30h

(g) t=9:00h (h) t=10:30h (i) t= 12:00h

Fig. 3.2: *Diffusion Test 2 with 2 ml/min injection speed as a function of time*

3.3 shows the results of Diffusion Test 3, the setup using four catheters. No improvement is seen compared to a mono injection-extraction catheter system. The contrast fluid is completely dispersed in the Petri dish after 3 hours. The fluid does not look completely homogeneous until after 9 hours. Figure 3.4 shows the results of Diffusion Test 4; a setup using lid-mounted catheters with an injection and extraction speed of 3 ml/min. The lid-mounted catheters show a lesser diffusion rate than the wall-mounted catheters. The contrast fluid does not move well towards the corners of the Petri dish. No full dispersion of the contrast fluid in the Petri dish is reached. the diagonal of the Petri dish does however show homogeneity after 12 hours.

3.1.2 Automatic Exchange in BC Culturing

Exchange Test 1 did not result in cellulose growth. The use of wall-mounted catheters was therefore discarded. Top mounted catheters were used instead. The visual results of test 2 to 5 can be found in Figure 3.5.

No BC patch formed on the surface of the medium in Exchange Test 1. Tiny BC strands attached to the glue around the catheters. An injection-extraction speed of respectively 2 and 1 ml/min, resulted in a thick but inhomogeneous cellulose patch in Exchange Test 2 [Figure 3.5A]. The patch is not layered. The wet thickness at the dense section is approximately 3 mm. Exchange Test 3; a faster injection-extraction speed of 3 ml/min with the exchange starting at the fifth day, resulted in an homogeneous result [Figure 3.5C]. However, BC was formed in

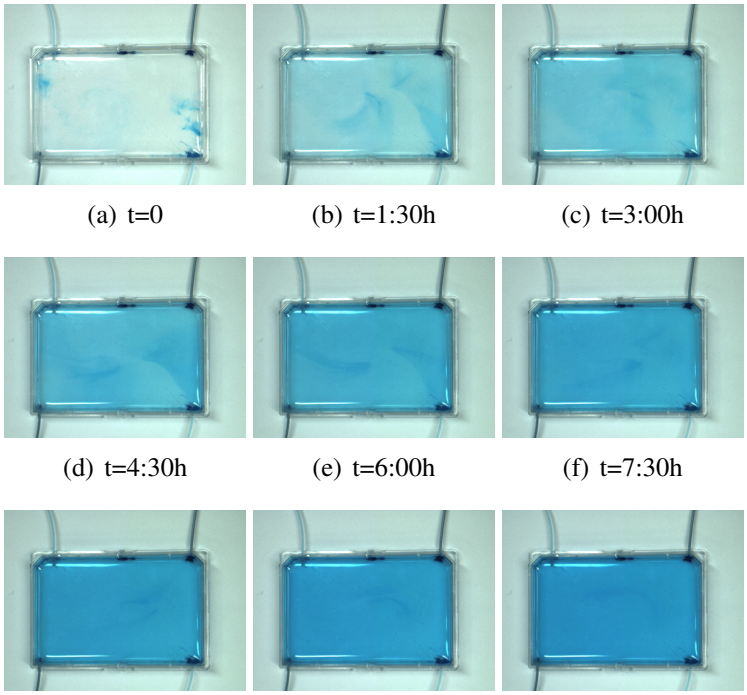

(a) t=0 (b) t=1:30h (c) t=3:00h

(d) t=4:30h (e) t=6:00h (f) t=7:30h

(g) t=9:00h (h) t=10:30h (i) t= 12:00h

Fig. 3.3: *Diffusion Test 3 with 1 ml/min injection speed, using four catheters, as a function of time*

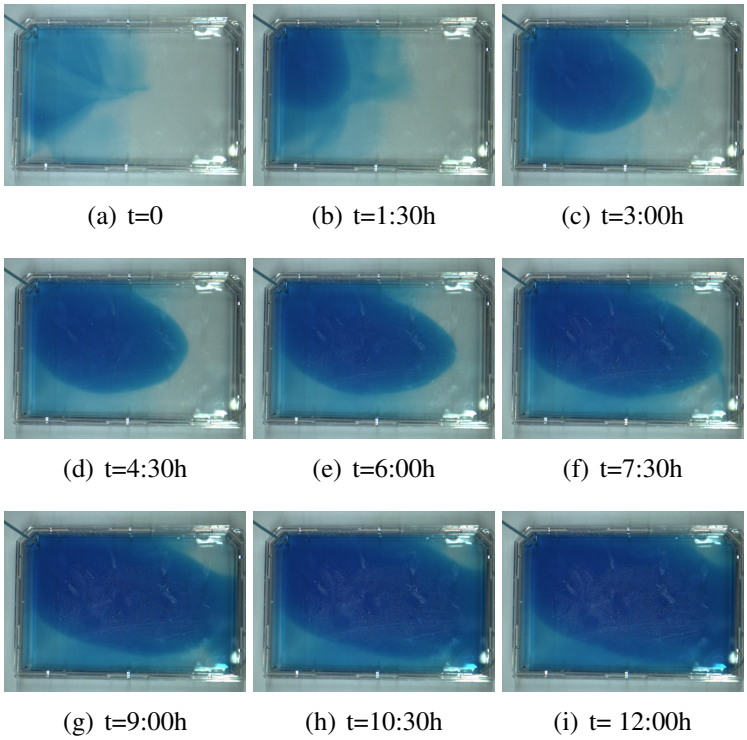

(a) t=0 (b) t=1:30h (c) t=3:00h

(d) t=4:30h (e) t=6:00h (f) t=7:30h

(g) t=9:00h (h) t=10:30h (i) t= 12:00h

Fig. 3.4: *Diffusion Test 4 with lid-mounted catheters and 2 ml/min injection speed as a function of time*

two layers. The wet thickness is approximately 2 mm. Exchange Test 4; A faster injection-extraction speed of 3 ml/min with the exchange starting at the third day, resulted in a thick but slightly irregular patch [Figure 3.5E]. The patch is not layered. The wet thickness is approximately 2 mm. Another test with identical conditions to Exchange Test 4, Exchange Test 5, resulted in a thick patch which is more regular than the Test 4 patch [Figure 3.5G]. However, it is not as homogeneous as the patch from Exchange Test 3. The patch is not layered. The wet thickness is approximately 2 mm. The black spot on the upper right originates from an air bubble stuck inside the BC during growth.

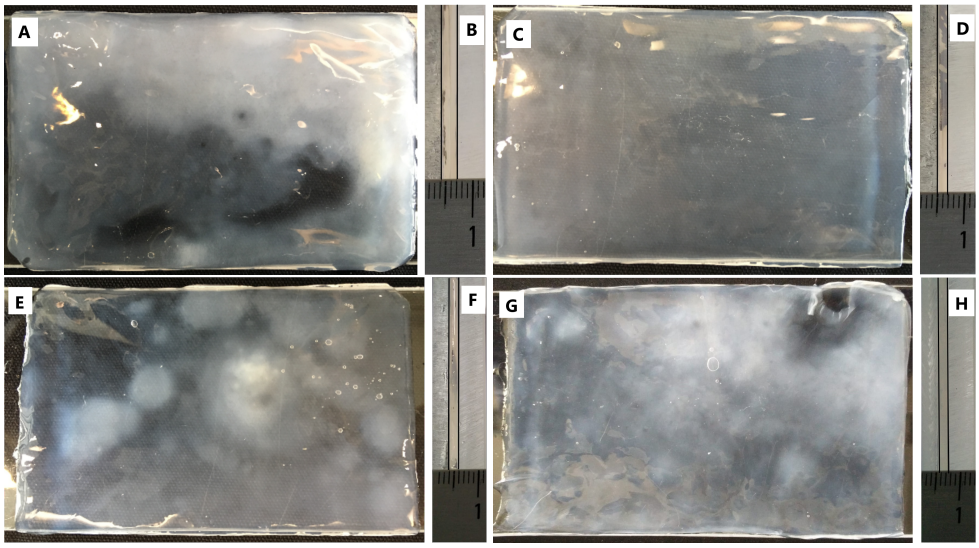

Fig. 3.5: *BC patches after 12 days of culturing with top-mounted catheter automatic exchange. Thicknesses are shown next to the patches. Lines have been added to improve contrast between the transparent BC and Plexiglas. (A) With an injection speed of 2 ml/min and extraction of 1 ml/min starting from the fourth day, (C) with a 3 ml/min injection speed starting from the fifth day, (E) with a 3 ml/min injection speed, starting from the third day and (G) the same as (E). (B), (D), (F) and (H) show the respective wet thickness of the patch*

Results of the characterisation of the BC patches can be found in Section3.3.

3.2 Rotary Culturing

3.2.1 Pilot study

The first test of the BC culture within the rotary device, Rotary Test 1, did not result in a feasible cellulose tube [Figure 3.6A]. The cellulose grew in threads over the stainless steel cylinder, but no real adherence of cellulose took place. The measured pH at the end of the culture period inside the box was 3.4. In Rotary Test 2, no feasible BC production took place [Figure 3.6B]. Bacteria seemed to adhere slightly to the cylinder, since a thin layer of BC was produced at the surface. It was however inhomogeneous, thin and very fragile. The measured pH inside the box at the end of the culture period was 3.5 In Rotary Test 3, BC formed on the surface of the cylinder [Figure 3.6C]. No difference in thickness could however be distinguished between BC grown on different material surfaces. Thick strings of cellulose formed around the cylinder.

Apart from the BC strings, the BC layer was very thin. No pH was measured. Rotary Test 4 resulted in a homogeneous layer of cellulose formed after three days [Figure 3.6D]. After six days, the cellulose started forming strings around the cylinder. After 11 days in the rotary device, the BC layer was thicker than in the three tests before. However, it did not form a tube and fell apart once touched.The measured pH inside the box at the end of the culture period was 3.6.

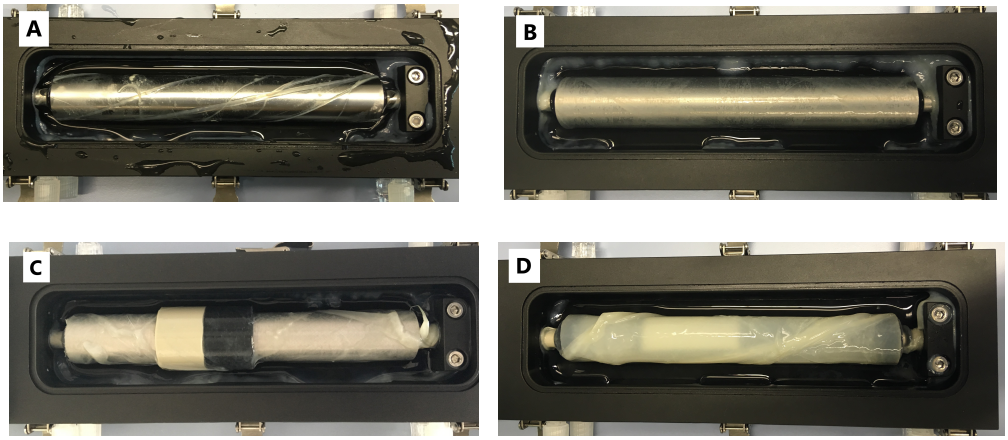

Fig. 3.6: *(A) Test 1 with the rotary device. Cellulose grew in strings around the cylinder. (B) Result of Test 2 with the rotary device. Cellulose grew, but as a thin and fragile layer. (C) Result of Test 3 with the rotary device. Cellulose grew well, but again in thick strings on top of a thin, fragile layer. (D) Result of Test 4 with the rotary device. The thickest layer of BC, although still fragile. Again, thick strings grew on the device as well.*

Appendix D shows further images of the material consistency for Rotary Test 2 and 4.

3.3 BC Characterisation

3.3.1 Density determination

SEM images have been taken of the sample from Exchange Test 2, and of the sample of Rotary Test 4. The micro-structure of BC cultured statically and rotational could therefore be compared. Figure 3.7 shows the micro-structure of the BC, at a magnification of x5500.

The results look surprisingly similar. The sample from the rotation Test shows thicker cellulose fibres, but less densely packed. Both images show interconnection of fibres. The images differ in contrast. The voltage was reduced for the Rotary Test 4 image in an attempt to fix this problem, but no similar contrast was attained.
The dark spot in the middle of Figure 3.7A is the area used for focusing. The area has been slightly burned due to a long exposure to the electron beam.

3.3.2 Strain testing

The inflation testing of the stationary cultured BC patches resulted in quiver plots, strain maps and pressure-strain graphs. All quiver plots display a zero shift point. The zero shift point is

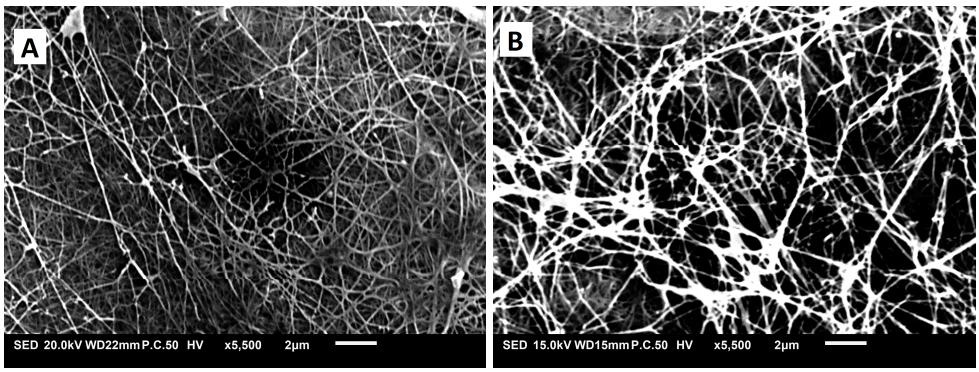

Fig. 3.7: *(A) A SEM image of the bacterial cellulose patch resulting from Exchange Test 2. (B) A SEM image of the bacterial cellulose patch resulting from Rotation Test 4: the silicon tube.*

defined as the point in the patch that stays exactly perpendicular to the camera. Many strain maps show compression near the edges.

The results of the pericardium patch are shown in Figure 3.8 [46]. It shows a very decentralised zero shift point in the quiver plots. The principle strain reaches about 0.015% after a pressure raise to 100 mmHg. Singularities are found at the edges of the patch. The strain is around zero after the pressure raise to 160 mmHg.

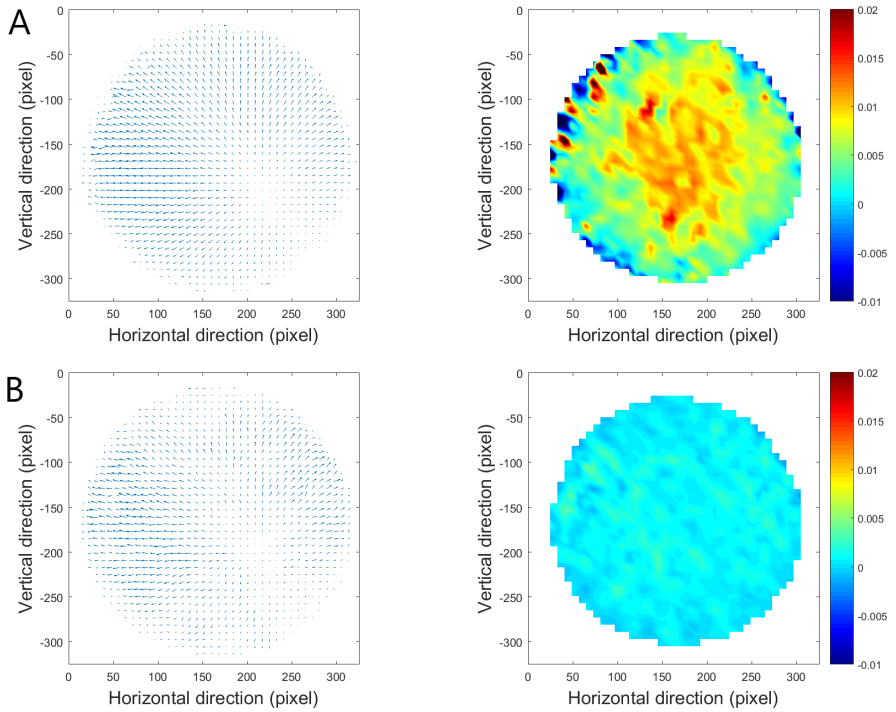

Fig. 3.8: *Quiver plot and strain map of the pericardium patch at (A) 100 mmHg and (B) 160 mmHg. Data adapted from [46]*

Figure 3.9 to Figure 3.16 show the quiver plot and strain map of the tested BC patches. The quiver plot shows that the zero shift point in the patch are not centralised for most patches.

Figure 3.9 shows the result of patch 1A. Patch 1A has been cut from the dense section of

the BC patch. The figure shows that the zero shift point of patch 1A is centralised until 100 mmHg, whereafter it moves slightly down and to the right. The dominantly blue strain map shows a very low strain in the patch through out the test. The patch experiences more strain going from 0 to 100 mmHg, as from 100 mmHg to 160 mmHg. The maximum principal strain lies around 1.5% after a pressure raise to 100 mmHg, while it is roughly zero after a pressure raise to 160 mmHg.

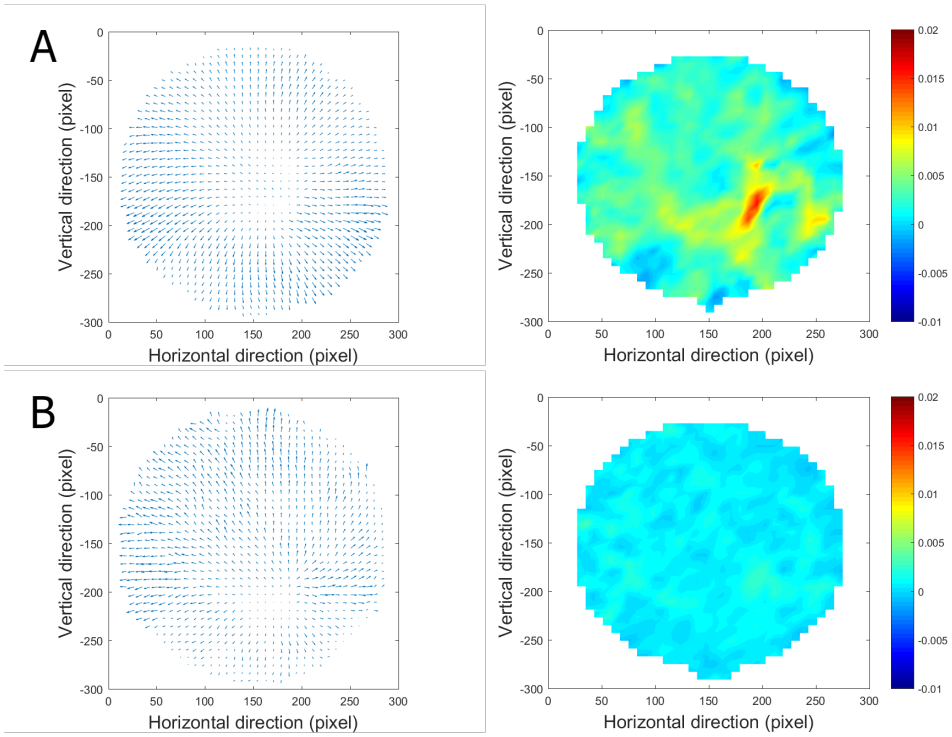

Fig. 3.9: *Quiver plot and strain map of the Test 1A BC patch at (A) 100 mmHg and (B) 160 mmHg.*

Figure 3.10 shows the quiver plot and strain map of patch 1B. The 1B patch has been cut from the scarcer section of BC of the Exchange Test 1 BC patch. The water column has not been raised to 160 mmHg. Again, the strain levels of the patch are relatively low, around 0.7% maximum principal strain. The zero shift point is centralised, as can be seen in the quiver plot.

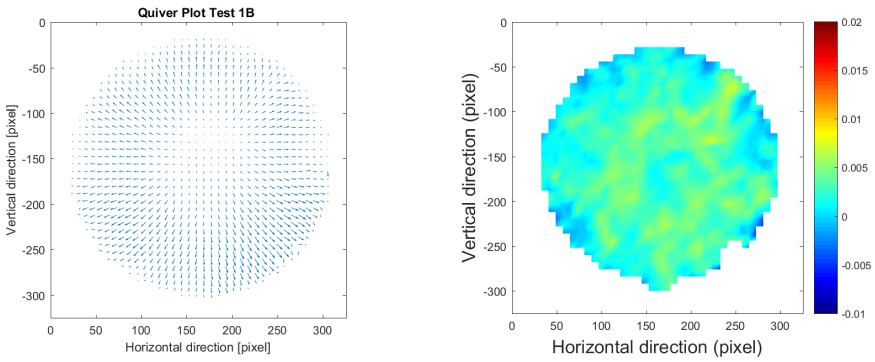

Fig. 3.10: *Quiver plot and strain map of the Test 1B BC patch at 100 mmHg.*

Figure 3.11 shows the results for the Test 2A BC patch. Again, no high strain level has been

measured. It is clear that localised high strains occur within the patch after a raise to 100 mmHg. These areas of high strains correspond to singularities in the quiver plot, and occur mostly near to the edges. One small point in the centre of the patch reaches a strain of around 3.0%. The surrounding areas do however not show a strain level above 2.0%.

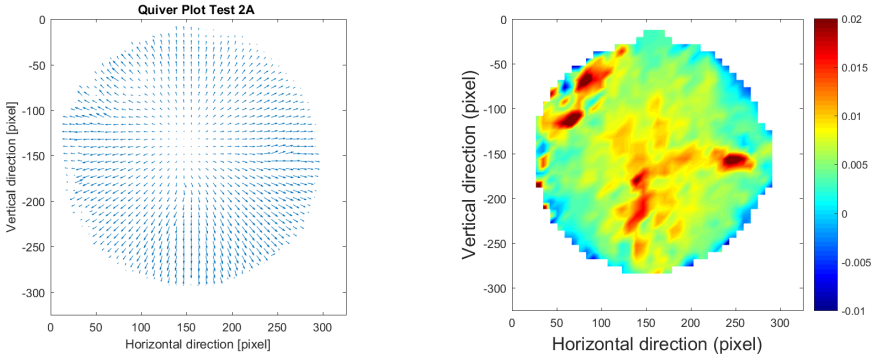

Fig. 3.11: *Quiver plot and strain map of the Test 2A BC patch at 100 mmHg.*

Figure 3.12 shows the quiver plots and strain maps of the Test 2B BC patch. It shows a low strain for both pressure levels, although the patch experiences more strain after a raise to 100 mmHg pressure. The zero shift point is almost centralised, but not completely. The central point also moves during the two pressure levels, going from the lower left corner to the a point slightly above centre. The maximum principal strain is approximately 1.0% after a raise to 100 mmHg, and around zero after a raise to 160 mmHg.

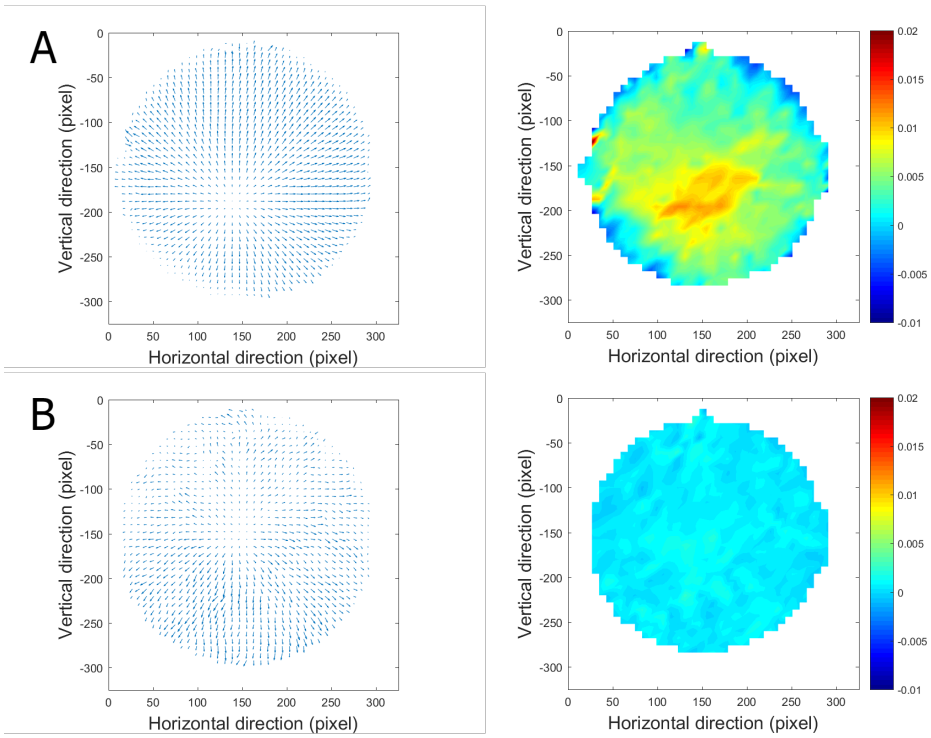

Fig. 3.12: *Quiver plot and strain map of the Test 2B BC patch at (A) 100 mmHg and (B) 160 mmHg.*

Figure 3.13 shows the results of the Test 3A BC patch. The corresponding quiver plot after

a raise to 160 mmHg shows large variations in deflection magnitudes throughout the patch. Both quiver plots seem quite centralised. The strain levels in the patch after a raise to 100 mmHg are relatively low compared to other patches, with a maximum principle strain around 0.7%. The strain levels in the patch after a raise to 160 mmHg are relatively high, also going to approximately 0.7% strain.

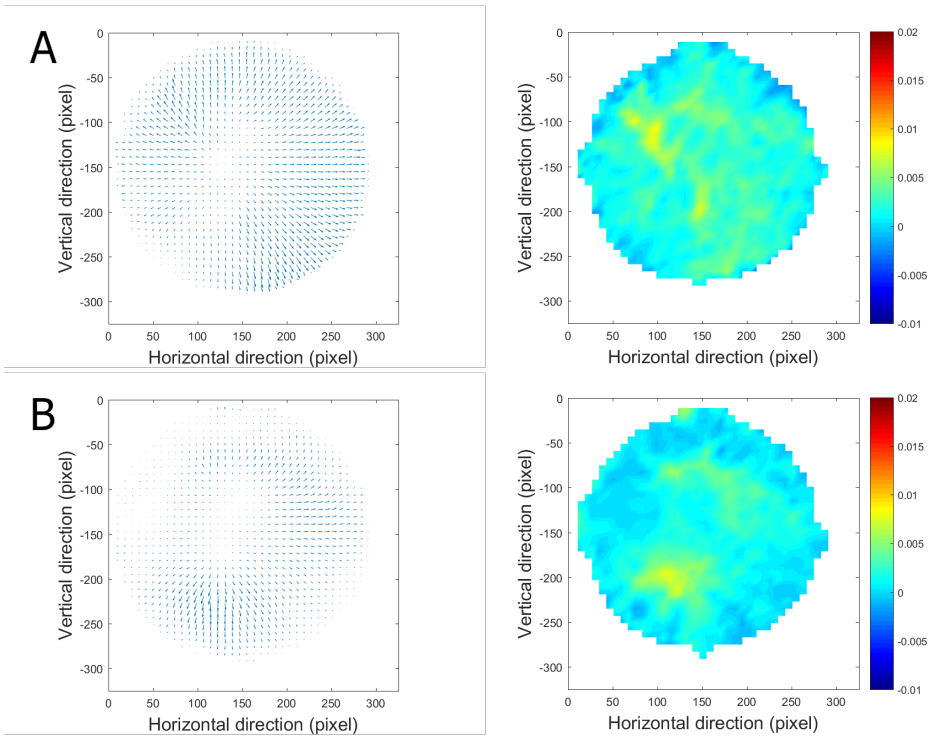

Fig. 3.13: *Quiver plot and strain map of the Test 3A BC patch at (A) 100 mmHg and (B) 160 mmHg.*

The quiver plots and strain maps of the Test 3B BC patch are shown in Figure 3.14. Looking at the quiver plots, the zero shift point is quite decentralised in the higher pressure level. After the pressure raise to 100 mmHg, the maximum principle strain is approximately 1.7%. This maximum strain lies however to the right of the patch, as opposed to more central. After a raise to 160 mmHg, the highest principal strain lies around 1.8%. This strain level is large compared to other patches after a pressure raise to 160 mmHg.

Figure 3.15 shows the results for the Test 4A BC patch.The zero shift point after the raise to 160 mmHg is not centralised. Overall, the strain levels are very low, both for the pressure raise to 100 and 160 mmHg. The highest principal strains after the raise to 100 mmHg lie around 0.6%. For the raise to 160 mmHg, the principle strain lie again around zero %.

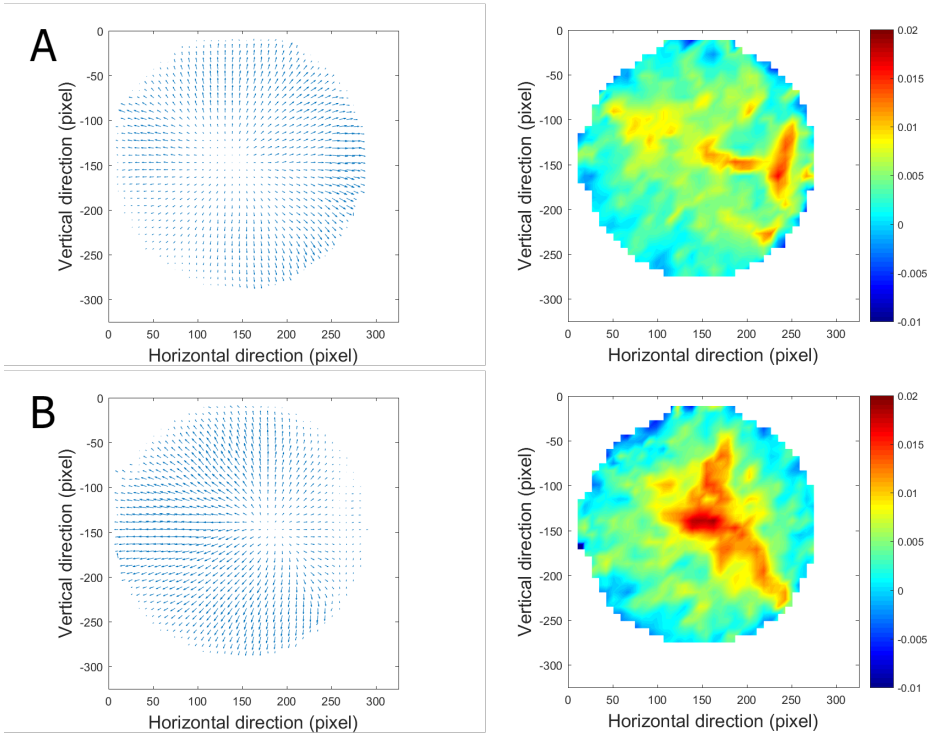

Fig. 3.14: *Quiver plot and strain map of the Test 3B BC patch at (A) 100 mmHg and (B) 160 mmHg.*

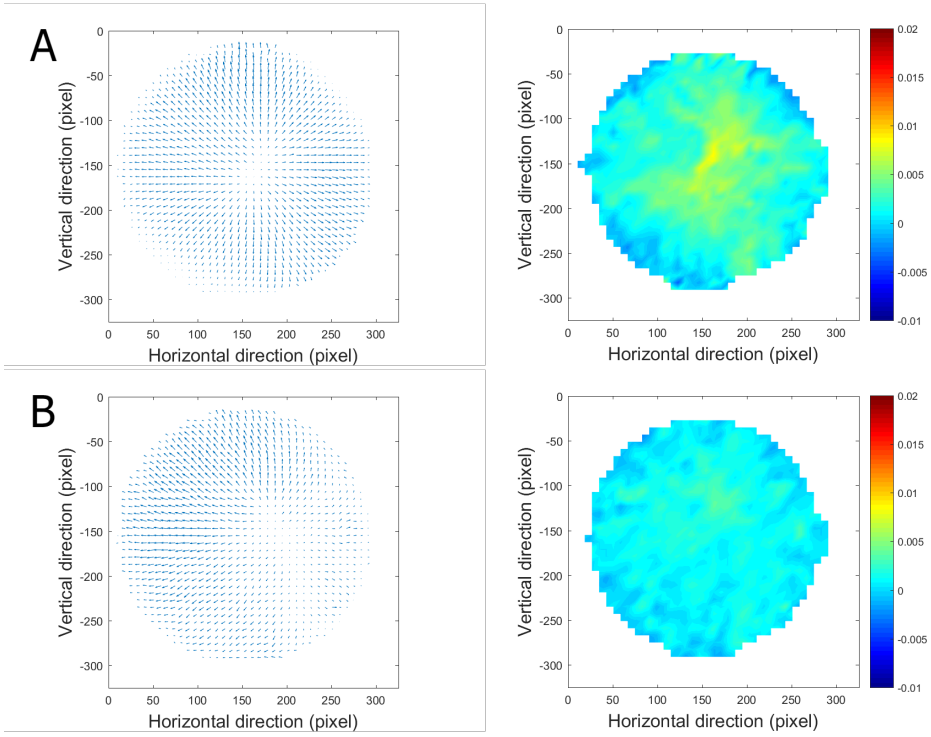

Fig. 3.15: *Quiver plot and strain map of the Test 4A BC patch at (A) 100 mmHg and (B) 160 mmHg.*

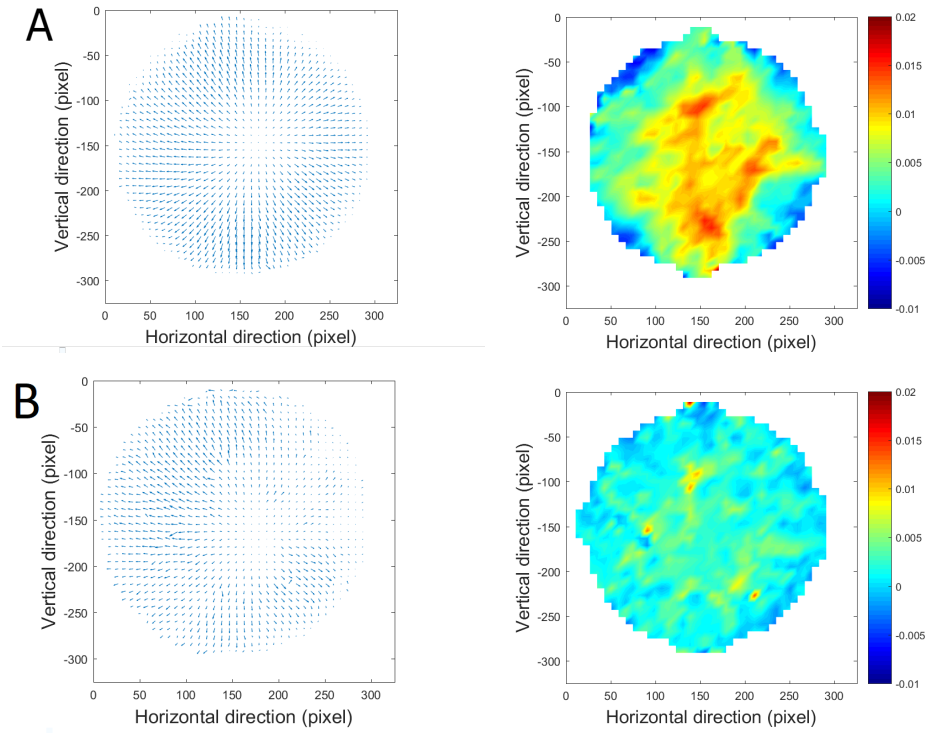

Fig. 3.16: *Quiver plot and strain map of the Test 4B BC patch at (A) 100 mmHg and (B) 160 mmHg.*

Figure 3.16 shows the quiver plots and strain maps of the Test 4B BC patch. The zero shift point is slightly decentralised, but does not move. A high principal strain of around 1.6% is present after a pressure raise to 100 mmHg. Slight strain is present after a raise to 160 mmHg, around 0.7%.
Comparing all results, it is clear that, except for patch 2A, all patches show similar strain levels after a raise to 100 mmHg. While patch 4B has similar high strains as the pericardium patch, all other patches (except patch 2A) show slightly lower strains after a pressure raise to 100 mmHg.

Patch 3A, 3B and 4B show higher strain levels than the pericardium patch after a pressure raise to 160 mmHg, with 4B having an exceptionally high strain level. Patch 1A, 2B and 4A show lower strain levels than the pericardium patch after a pressure raise to 160 mmHg.

Table 3.1 shows a summary of the results.
Figure 3.17 shows the average principle strains at measured pressure points for the pericardium patch. A curve has been fitted through the data points. The equation used to fit through the data points of the pericardium patch, and patch 3A to 4A, is an exponential resembling the function for a normal distribution:

$$\frac{a}{b} \cdot e^{-b \cdot x^2} - \frac{a}{b}$$

The data points for patch 1A to 2B have been fitted with a curve of the equation:

$$a \cdot e^{b \cdot x} - a$$

Figure 3.18 shows these graphs for all other measured BC patches. The data follows the typical curve of an elastic material: relatively small pressure is needed to strain the material, but as the

pressure rises, the material becomes stiffer. The pericardium patch and patches 3A to 4B show a slight flattening of the curve as the pressure keeps increasing.

Tab. 3.1: *BC and pericardium patch strain levels at a pressure level of 100 mmHg and 160 mmHg.*

Pressure level [mmHg]	Patch	Average Principal Strain [%]
100	Pericardium patch	0.9
	Patch 1A	0.42
	Patch 2A	0.8
	Patch 2B	0.7
	Patch 3A	0.3
	Patch 3B	0.6
	Patch 4A	0.45
	Patch 4B	0.85
160	Pericardium patch	0.99
	Patch 1A	0.47
	Patch 2B	0.9
	Patch 3A	0.57
	Patch 3B	1.4
	Patch 4A	0.64
	Patch 4B	1.62

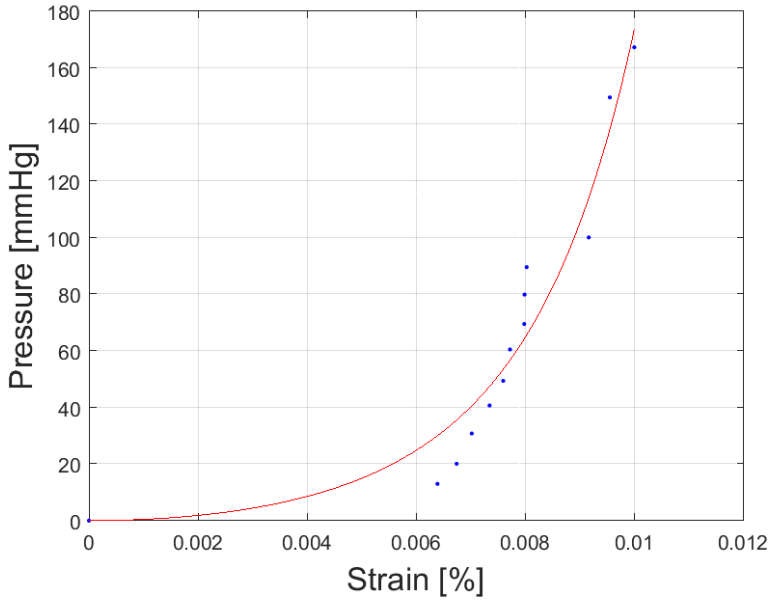

Fig. 3.17: *Pressure vs. Strain graph of the average principal strain for the pericardium patch. Data adapted from [46].*

Figure 3.19 shows all curves in one figure. The pericardium patch shows higher strain levels as compared to almost all BC patches.

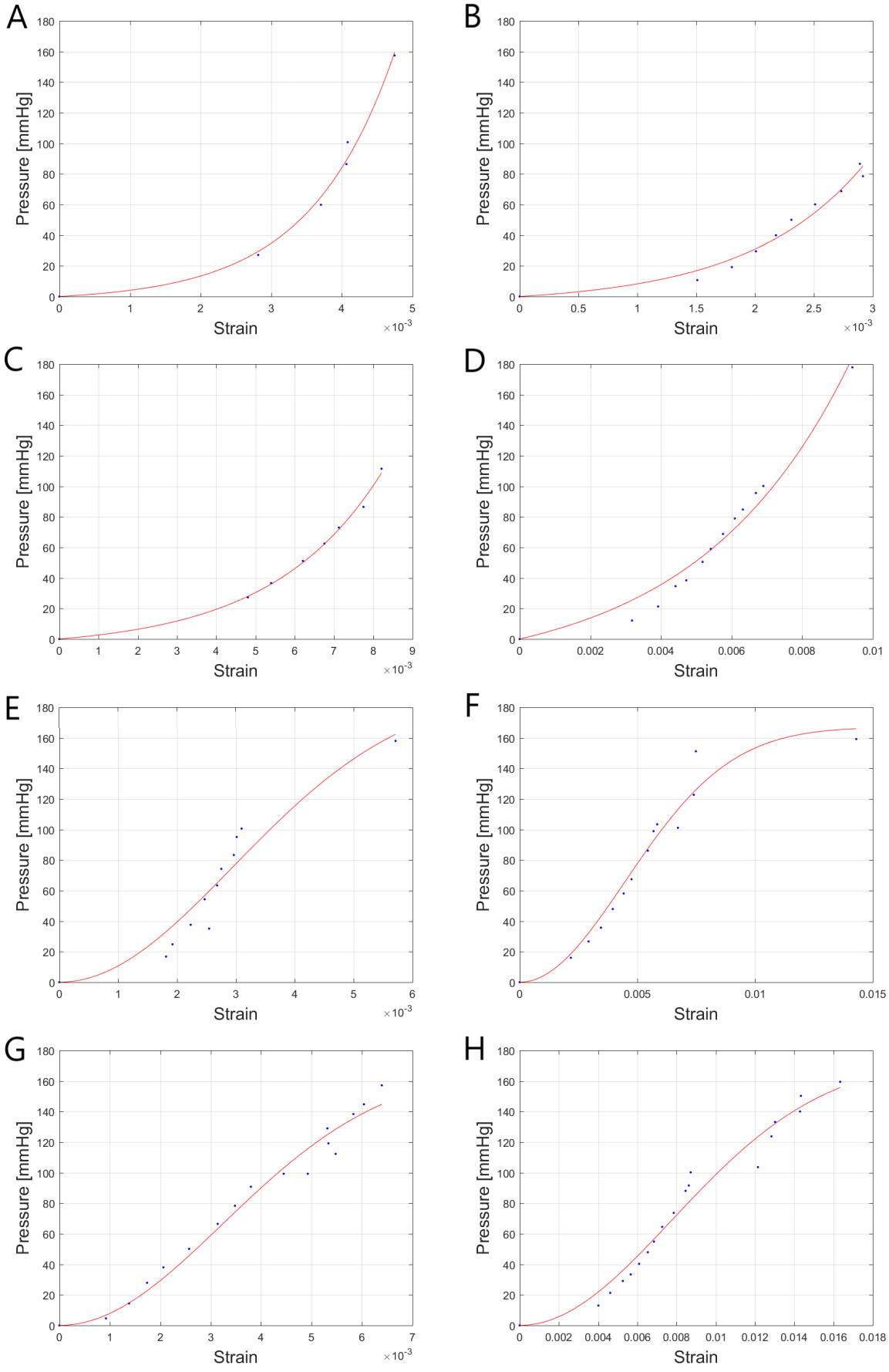

Fig. 3.18: *Pressure vs. Strain graph of the average principal strain of all BC patches. (A) Patch 1A, (B) patch 1B, (C) patch 2A, (D) patch 2B, (E) patch 3A, (F) patch 3B, (G) patch 4A, (H) patch 4B.*

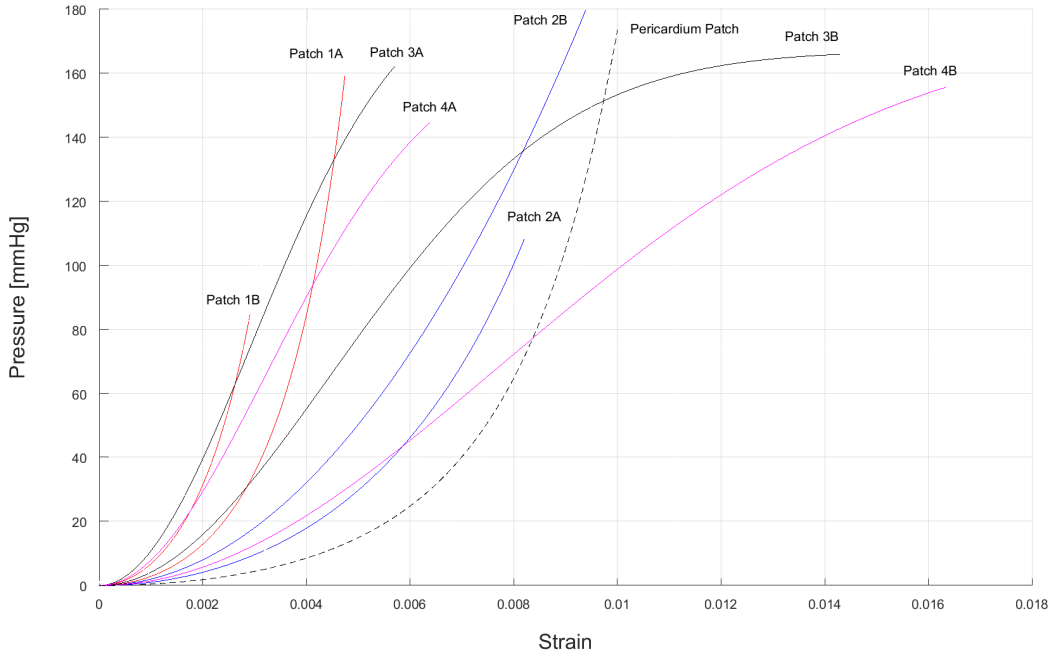

Fig. 3.19: *Total overview of all Pressure vs. Strain graphs*

3.3.3 Creep testing

The results of the creep tests at 100 mmHg are shown in Figure 3.20 . Figure 3.21 shows the results of the creep testing at 160 mmHg. For BC patch 1A and 1B, no creep tests have been performed. Most creep tests show a fast creeping behaviour in the first 100 to 200 seconds, after which the curve flattens or rises more gradually. It is clear that the creep tests contain large amounts of noise, since no clear curve can be distinguished.

In the 100 mmHg creep tests, patch 2A shows a curve that rises fast in the first 300 seconds, and then flattens out [Figure 3.20A left]. After 300 seconds, the data has only been captured at 1 data point per minute, making the curve look relatively scarce. After 300 seconds, the patch stays at a strain level of approximately 0.053%.

Patch 2B shows a curve differing from the other patches [Figure 3.20A right]. the creep level rises slowly, after which is starts descending after 600 seconds. The strain level levels at a value of roughly 0.49%.

Patch 3A shows a steep increase in strain during the first 200 seconds, after which the curve flattens at around 0.1% strain [Figure 3.20B left].

Patch 3B shows a curve that does not level out after 20 minutes of creep testing [Figure 3.20B right]. The strain level keeps increasing, having a value of around 0.14% after 20 minutes. A steeper increase is present in the first 100 seconds.

Patch 4A shows a curve with steep increase in strain during the first 100 seconds [Figure 3.20C left]. The curve flatten out at a strain level of around 0.11%.

Patch 4B shows similar behaviour to patch 3B [Figure 3.20C right]. The curve has a steep increase in strain levels in the first 400 seconds, after which the strain level keeps increasing slowly. After 20 minutes, the patch reaches a strain level of around 0.27%.

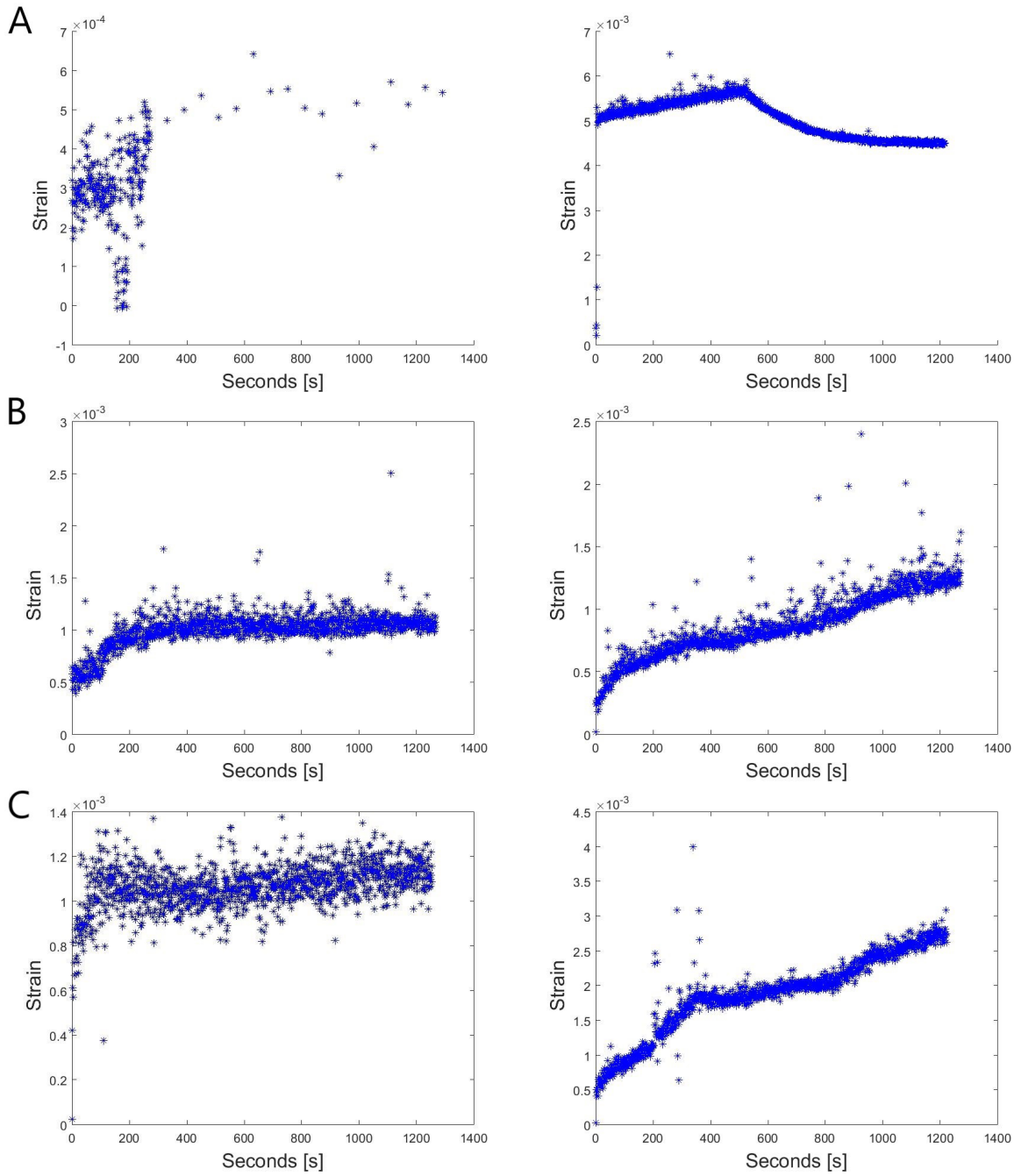

Fig. 3.20: *Results of creep testing for 20 minutes at a pressure of 100 mmHg. (A) Patch 2A (left) and Patch 2B (right). (B) Patch 3A (left) and Patch 3B (right). (C) Patch 4A (left) and Patch 4B (right)*

Figure 3.21 shows the creep tests at a pressure level of 160 mmHg. Patch 2A data was not usable.

Patch 2B shows no real steeper strain increase in the first seconds [Figure 3.21A]. The curve keeps increasing slowly during 20 minutes, ending at a strain level of approximately 0.05%.

Patch 3A shows a steep strain increase in the first 50 seconds [Figure 3.21B left]. The curve flattens out at a strain level of approximately 0.1%.

Patch 3B shows a steep and large strain increase in the first 50 seconds [Figure 3.21B right]. The curve does not flatten out, and keeps increasing gradually. After 20 minutes, a strain of

approximately 0.99% is reached.

Patch 4A shows an initial steeper increase that gradually flattens, instead of a steep increase that abruptly changes to a gradual slope [Figure 3.21C left]. The curve remains relatively steep for the first 400 seconds, after which it flattens at a strain level of around 0.12%.

Patch 4B has a steep slope until 400 seconds, after which it flattens out at around 0.2% strain [Figure 3.21C right].

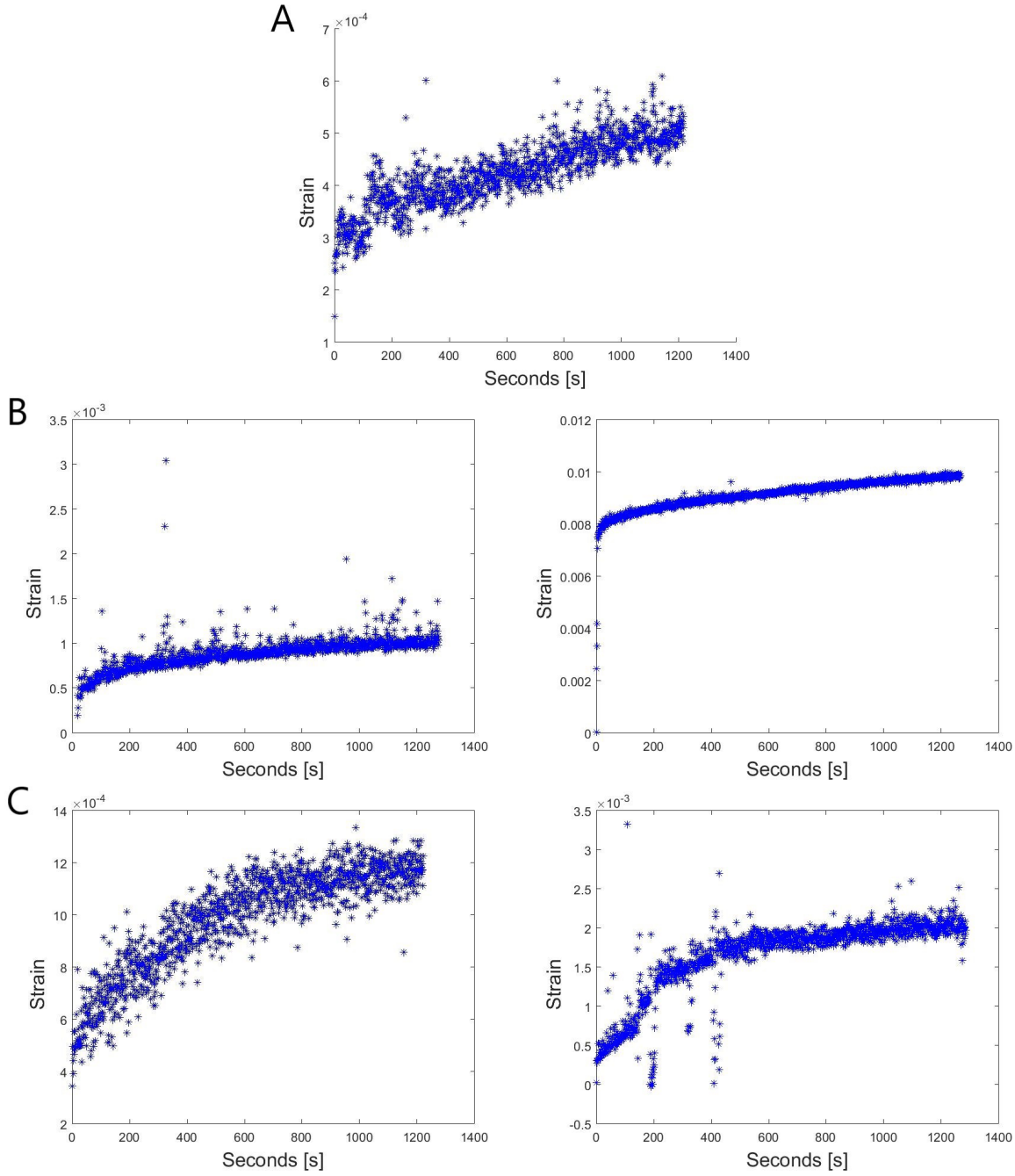

Fig. 3.21: *Creep over 20 minutes at a pressure of 160 mmHg. (A) Patch 2B. (B) Patch 3A (left) and Patch 3B (right). (C) Patch 4A (left) and Patch 4B (right)*

These results have been summarised in Table 3.2. There is no clear difference in strain levels at different pressures. The strain level increases for patch 3B, while it decreases for patch 2B.

The other patches keep roughly the same strain levels.

Tab. 3.2: *Results of the creep testing of 20 minutes of the BC patches at a pressure level of 100 mmHg and 160 mmHg.*

Pressure level [mmHg]	Patch Number	Final Strain [%]	Time to level [s]
100	Patch 2A	0.053	300
	Patch 2B	0.49	-
	Patch 3A	0.1	200
	Patch 3B	0.14	-
	Patch 4A	0.11	100
	Patch 4B	0.27	-
160	Patch 2B	0.05	-
	Patch 3A	0.1	50
	Patch 3B	0.99	50
	Patch 4A	0.12	400
	Patch 4B	0.2	400

Chapter 4

Discussion

The results of static culturing, rotary culturing, density testing, strain and creep testing will be discussed in the following chapter. The discussion will focus on the feasibility of BC for the use as a biomaterial for prosthetic heart valves.

4.1 Static Culturing

4.1.1 Diffusion Pilot study

The diffusion test show a clear superiority of wall mounted catheters. The colouring fluid easily disperses throughout the complete Petri dish, almost independent of injection speed or catheter number. However, due to their inefficacy in BC culturing, the wall-mounted catheters had to be discarded.

4.1.2 Automatic Exchange in BC Culturing

Exchange Test 1 did not result in BC growth. It is hypothesised that the glue used for fixating the wall-mounted catheters, was the cause for the lack of bacteria activity. Culturing with lid-mounted catheters namely did result in BC growth.

Exchange Test 2 clearly shows the inhomogeneous dispersion of the medium under the Patch. BC grew much denser and thicker on one diagonal of the patch, than on the other diagonal. A faster injection speed is therefore beneficial. Exchange Test 3 indeed shows that a faster injection speed produces much better medium dispersion, and therefore more homogeneous patches. However, the patch consisted out of two layers. The layers were most likely formed by the late start of the exchange. Exchange Test 4 did not show layering, indicating that the exchange should indeed be started at an earlier time. Exchange Test 5 also did not show layering, but does not look equal to the patch from Exchange Test 4. This test indicates that the growth process is still sensitive and hard to perfectly reproduce. The patch from Exchange Test 5 also shows a slightly denser BC growth on one diagonal of the patch, similar to Exchange Test 2. This indicates that the injection speed might still not be optimal.

The wet thicknesses of the patches seem reproducible; 2 mm for all patches except Exchange Test 2. Exchange Test 2 produced a patch with a maximum thickness of 3 mm, but this result was not homogeneous.

2 mm (1-2.7mm)is also the wet thickness reached by many patches produced in [46], having been cultured for 12 days with medium exchange every third day. The maximum thickness

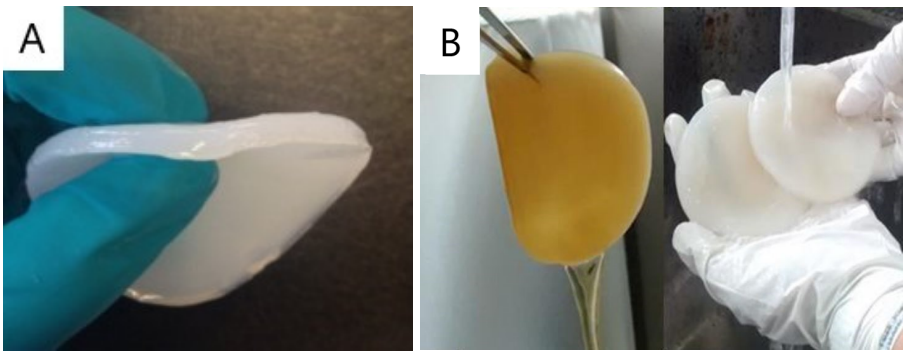

Fig. 4.1: *(A) Culture for 7 days, resulting in 3 to 5 mm thick patches [24]. (B) Culture of Acetobacter Hansenii 10 days [10]*

reached in previous research ([58]) with the same protocol as in [46], resulted in patches with thicknesses around 2 mm, going up to 2.9 mm.

Looking at literature, this thickness seems low. For example, Krystynowicz produced patches with a thickness of 1.25 cm after culturing for 7 days without medium exchange [37]. Figure 4.1 shows several other results from literature. Opposite results can also be found; Chanliaud finds a BC patch thickness of 0.35 mm after culturing for 3 days [7]. The main differences between literature and the current research protocol, are the use of different media and the addition of oxygen. As has been stated by Bodin et al. [5], addition of oxygen decreases patch thickness, but increases patch density. The thickness of the patch is therefore not a marker for patch quality.

The ultimate goal of the automatic exchange tests was to produce BC patches without layers (as seen in [58]). This goal has been accomplished, since the patches from Exchange Test 2, 4 and 5 did not show layering.

4.2 Rotary Culturing

Rotation Test 1 did not result in a cellulose tube; the BC did not attach to the smooth stainless steel surface. This behaviour has also been observed by Lin et al. [38]. Lin et al. states that the stainless steel surface is too smooth for BC attachment, although some BC actually did attach in their experiments. Figure 4.2A shows their results.

These tests differ from the current research method in their rotator size and shape. This might be a determining factor in the growth process of the BC.

Rotation Test 2 was hypothesised to provide better attachment, since the used silicon is rougher than stainless steel. The BC structure was similar to that of BC growing without a proper supply of oxygen (observed in previous research), and to BC that is limited in growth due to the presence of toxic substances (observed in Exchange Test 1).

Rotation Test 3 did not yield a BC tube. Polyethylene and polypropylene were hypothesised to result in better attachment, since these materials have been used successfully in literature. Figure 4.2B and C show such results. The rougher stainless steel was also hypothesised to provide better attachment, since this was stated by Lin et al. [38]. The BC did look more promising than the BC from Rotation Test 1, but did not produce the desired result. No difference could be seen between different surfaces. BC grew similar on every surface. The rotator size and shape is again a difference between the rotator protocols used in literature.

Fig. 4.2: *Results on industrial rotation devices of (A) Lin et al. [38] on stainless steel for five days, (B) Kim et al. [34] on polypropylene for four days and (C) krystynowicz et al. [37] on polyethylene for seven days*

Rotation Test 4 did not produce a BC tube, although thick strands of BC grew on the tube. The silicon tube was hypothesised to produce better BC, since a BC tube had grown on the same material in an earlier test with the same material, but a smaller tube (Appendix D). The size of the tube might be a factor for the low BC growth level.

The pH of the medium at the end of each test stayed low, even though injection speed was increased and interval time lowered. This low pH can be detrimental for BC growth, and might therefore well be a cause for the lack of tubular formation.

Bodin et al. [4] used the same technique as the current research method, and reported growth of BC. Bodin et al. however grew a smaller size tube, on different material. Furthermore, they reported a different method to be superior to the semi-submersed rotator method. Namely, a completely submersed, air-permeable, rotator. A quick feasibility test of this method is presented in Appendix E. Rotation speed and submersion level have not been systematically investigated. These factors might also change BC growth.

4.3 Density Determination

Images were taken of all BC samples. The quality of the images is however not high enough to quantitatively determine patch density. It is hypothesised that the used coating of the material was the cause for the lesser quality of the SEM images. Different sections of the patches also displayed different fibre densities, making it impossible to compare patch densities with only one image per patch.

The images in Figure 3.7 show thicker fibres for the BC from Rotation Test 4, than for the BC from Exchange Test 2. It also shows larger pores. These differences can however stem from a difference in voltage or contrast.

The images do show the structure of the BC. It is indeed of a fibrous nature, with large pores. Fibres are interconnected and unaligned, resulting in homogeneous mechanical properties in all directions. The SEM images correspond to SEM images found in literature [26], having the same fibre thickness.

4.4 Strain Testing

It is clear that BC is an elastic material that increases in stiffness as the material stretches. Both the strain maps and pressure vs. strain graphs show this behaviour. The stiffness increase

is linked to the alignment of fibres inside the material. When the fibres are not aligned, the material stretches easily as the fibres move. When the fibres are completely straight, they start to stretch themselves, greatly increasing the stiffness of the material [40].

Contrary to many BC patches cultured by Andrea Nienhaus [46], the patches from Exchange Test 1 to 4 did not rupture during testing. This leads to the conclusion that the automatic exchange protocol indeed improves the stability and strength of the BC patches, compared to manually exchanging the medium every third day. The average principal strain at a pressure of 80 mmHg of the BC patches from Exchange Test 1 to 4 is 0.5% (SD: 0.21%). Visual inspection of the strain maps of BC patches by Andrea Nienhaus, shows that 2 of the measured BC patches also have an average strain level of 0.5%. One patch shows higher strain levels, going up to an average of 2%, while another shows lower strain levels of 0.3%. No significant change is therefore present between the stiffness of the BC patches from Exchange Test 1 to 4, and the BC patches by Andrea Nienhaus [46].

The pericardium patch shows an average principal strain of 0.84% at 80 mmHg. This strain is higher than almost all BC patches from Exchange Test 1 to 4 show. A too stiff material is not beneficial for the function of a heart valve. However, the stiffnesses of the pericardium patch and the BC samples still lie in the same range. The strain level found by Chanliaud et al. at a pressure of 80 mmHg, was approximately 0.9% [7]. The strain levels measured in this research are therefore similar to literature.

The thick section of Exchange Test 1, patch 1A, shows a higher strain than almost all other tested BC patches. The thin section of Exchange Test 1, patch 1B, actually shows the lowest strain level. These results are counter intuitive, but no definitive conclusion can be drawn about the thickness-stiffness relation, due to the small sample size.

The compression at the edges of the BC patches can be explained by the out-of-plane movement of the edge of the patch. The deflection in z-direction of the patch edge is recognised by the PIV program as a compressive strain, since particles seem to be moving closing together.

4.5 Creep Testing

Most creep graphs display the viscoelastic nature of the BC material. Application of a constant pressure causes a slow increase in strain in the material, until the strain levels do not rise anymore and level out. The slow rise in strain is caused by fluid redistribution through pores within the BC fibrous network [40]. This redistribution takes time, giving rise to the creep behaviour shown in Figures 3.20 and 3.21.

The creep graphs are extremely noisy. The noise is most likely caused by pressure level variations. The water influx during creep testing keeps the pressure level semi-steady, but a completely steady pressure level was not attainable. Pressure levels varied from 159 to 161 mmHg.

Some patches show a continuously rising strain level. It is hypothesised that these patches will also show a constant strain level after creep testing for a longer period of time.

Creep tests were performed on BC by Chanliaud et al. [7]. No time-dependency was apparent. However, Chanliaud et al. also tested other materials, which had extremely time-dependent behaviours. Relative to those materials, BC did not show a time-dependency.

Human pericardium tissue has been tested by Lee et al. [45]. They found a 0.3% strain increase after 30 minutes at a pressure of 60 mmHg. For a material under cyclic loading, this creep level is insignificant. Although patch 2B and 3B show higher strain levels after testing

at respectively 100 and 160 mmHg, most patches have strain levels lower than 0.3% strain. If, after testing a larger sample size, it is found that BC does indeed not creep more than 0.3%, the creep of the material can also be deemed insignificant.

Conclusions and Recommendations

4.6 Conclusion

In conclusion, the BC cultured with the novel method of automatic medium exchange, is more stable and stronger than patches cultured with the previous culturing protocol. However, BC cultured using the rotary device is unstable and fragile. The rotary culturing protocol needs to be improved in order to result in feasible BC tubes for the production of heart valves.

The BC shows strain levels slightly stiffer, but relatively similar to those of human pericardium. Furthermore, creep behaviour is, as with pericardium, insignificant under cyclic loading conditions.

More patches need to be cultured in order to increase the sample size, and thereby produce more conclusive results. The results already gathered in this master thesis research, show that BC material has promising mechanical characteristics, possibly rendering it a feasible option for the use in bioprosthetic heart valves.

4.7 Recommendations

The pilot exchange test showed significantly better diffusion with wall-mounted catheters. Experiments should therefore be conducted to introduce catheters trough the Petri dish walls without using the toxic glue. If no solution can be found, introducing two extra catheters (similar to Diffusion Test 3) trough the lid of the Petri dish could also improve diffusion.

The thicker patches in different literature sources leave the question whether the current production protocol is optimal. The author advises to firstly test different available media for Acetobacter Xylinus.

Increasing the pH of the medium inside the rotation device is paramount in order to be able to give the BC an optimal growth environment. Faster injection speeds or different media (i.e. sucrose instead of glucose [52] [13]) could solve this problem.

Materials with better surfaces for bacterial attachment are needed for the production of a BC tube. Different options used successfully in literature are Gore-Tex ([4]), or the use of a mesh ([47], [56]).

The effect of different rotation speeds and different submersion levels should be investigated. The concept of completely submersing the rotator and letting air run trough it, could also be tested.

To better quantify density of the material, SEM images need to be taken with better quality. Coating should be improved to improve the quality. More time is needed to calibrate the SEM and thereby create better images.

To apply statistics to the outcome of strain and creep testing, more samples will need to be produced and tested. This will result in more definitive conclusions on the material properties

and the production method reproducibility.

Images have been taken of the side of the patches. These images can be processed to yield 'deflection height vs. pressure' graphs. Using the method presented by Elsheikh& Anderson [17], these graphs could potentially be converted into 'stress vs. strain' graphs. These graphs and the Young's Modulus resulting from these graphs can be used to better compare the BC properties with literature and other materials.

Not all creep experiments resulted in typical viscoelastic creep curves. The creep test for patch 3B and 4B at 100 mmHg, and the creep test for patch 2B and 3B at 160 mmHg, do not level out. Longer creep tests will need to be conducted in order to see the final level of strain after it has levelled out.

The viscoelastic behaviour of the material will most likely change at different temperatures. Testing at body temperature would give a better insight in the BC material properties when implanted inside the heart.

The noise during creep testing could be reduced by designing a test set-up that is either hermetically tight, or allows for extremely steady and precise water influx.

A creep modulus can be defined if more creep tests are conducted at different stress levels. The creep modulus can give better insight into the creep behaviour of the BC at different pressure levels.

Appendix A

Agar and Medium Composition

ATCC medium: 459 YGC medium

Glucose.....50.0 g
Yeast extract.....5.0 g
$CaCO_3$.....12.5 g
Agar.....15.0 g
Distilled water.....1.0 L

Autoclave at 121C for 15 minutes.

Fig. 1.1: *AGAR composition as dictated by the ATCC*

Acetobacter Xylinum

Medium mit Glucose 2.381% zur Zelluloseproduktion

				Ansatz g /		Ansatz mg /						
		Prozent	MW	1 L	2 L	1 L	2 L	4 L	5 L	4 L	5 L	MilliQ H_2O
KH_2PO_4	Kaliumdihydrogenphosphat	0.7		7.00 g	14.00 g			28.00	35.00			
MgSO4 ~~$MgSO_4$ x 7 H_2O~~	Magnesiumsulfat Heptahydrat	0.213		~~2.13 g~~	~~4.26 g~~	1.040g	2.081g	8.52	10.65			
H_3BO_3	Borsäure	0.00043		0.0043	0.0086	4.3 mg	8.6 mg	0.0172	0.0215	17.2 mg	21.5 mg	
Nicotinamide		0.00007		0.0007	0.0014	0.7 mg	1.4 mg	0.0028	0.0035	2.8 mg	3.5 mg	
$FeSO_4$ x 7 H_2O	Eisensulfat Heptahydrat	0.00095		0.010	0.019	9.5 mg	19.0 mg	0.038	0.0475	38.0 mg	47.5 mg	
Na_2HPO_4	Di-Natriumhydrogenphosphat	0.134	142	1.34 g	2.68 g			5.36	6.70			
$(NH_4)_2SO_4$	Ammoniumsulfat	0.354		3.54 g	7.08 g			14.16	17.70			
Ethanol abs		0.473		4.73 ml	9.46 ml			18.92	23.65			
Glucose 50%		2.381		50.0 ml	100.0 ml	Ansatzart Beispiel: In 1 L Salzlösg. 50 ml Glucoselösg. geben						

Glucose 50% ansetzen: 500 g / 1000 ml MilliQ H_2O, sterilfiltern.

Die Salzösung ansetzen, über Nacht im Kühlraum lagern. Ethanol direkt vor dem Autoklavieren zugeben. Die 50% Glucoselösung nach dem Autoklavieren, vor Gebrauch, in das **RT warme** Medium geben.

1) form glucose 50% solution, sterile filter
2) mix remaining salts in MilliQ and store overnight in fridge
3) add ethanol just before autoclaving, autoclave
4) add glucose solution after autoclaving to RT medium (just before using)

Bestandteile	Herkunft
KH_2PO_4	Kaliumdihydrogenphosphat purum, Fluka, Artikel Nr. 60230
$MgSO_4$ x 7 H_2O	Magnesiumsulfat Heptahydrat, Fluka, Artikal Nr. 63142
H_3BO_3	Borsäure, Fluka, Artikal Nr. 15660
Nicotinamide	Nicotinamide, cell culture tested, Sigma, Artikel Nr. N0636-100G
$FeSO_4$ x 7 H_2O	Eisensulfat Heptahydrat, Sigma, Artikel Nr. F8633-250G
Na_2HPO_4	Di-Natriumhydrogenphosphat, Sigma, Artikel Nr. S3264-500G
$(NH_4)_2SO_4$	Ammoniumsulfat, Fluka, Artikel Nr. 09980
Ethanol abs	Ethanol absolut (>99.8%), Fluka, Artikel Nr. 02860
Glucose	D(+)Glucose wassserfrei, Sigma, Artikel Nr. 16325

Fig. 1.2: *Culture Medium used for the production of BC by Acetobacter Xylinum*

Appendix B

Technical Drawings of Inflation Device

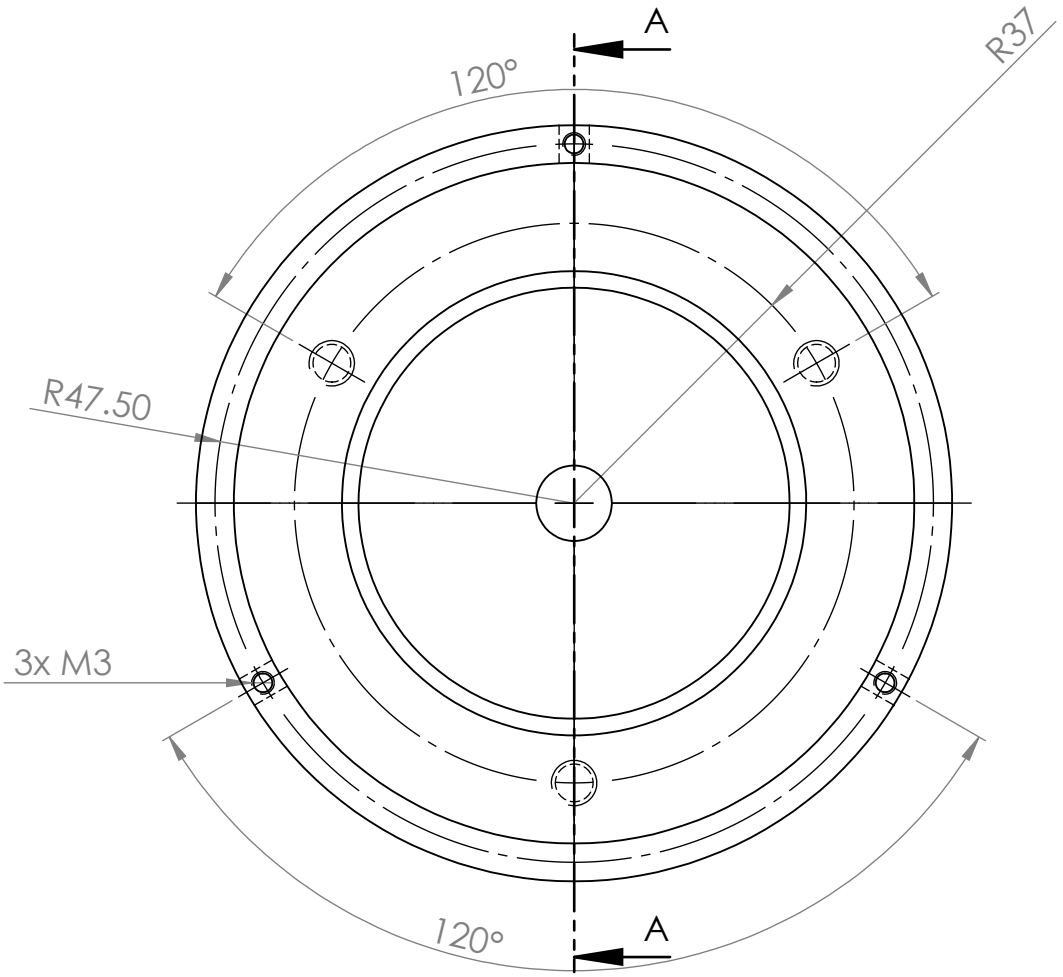

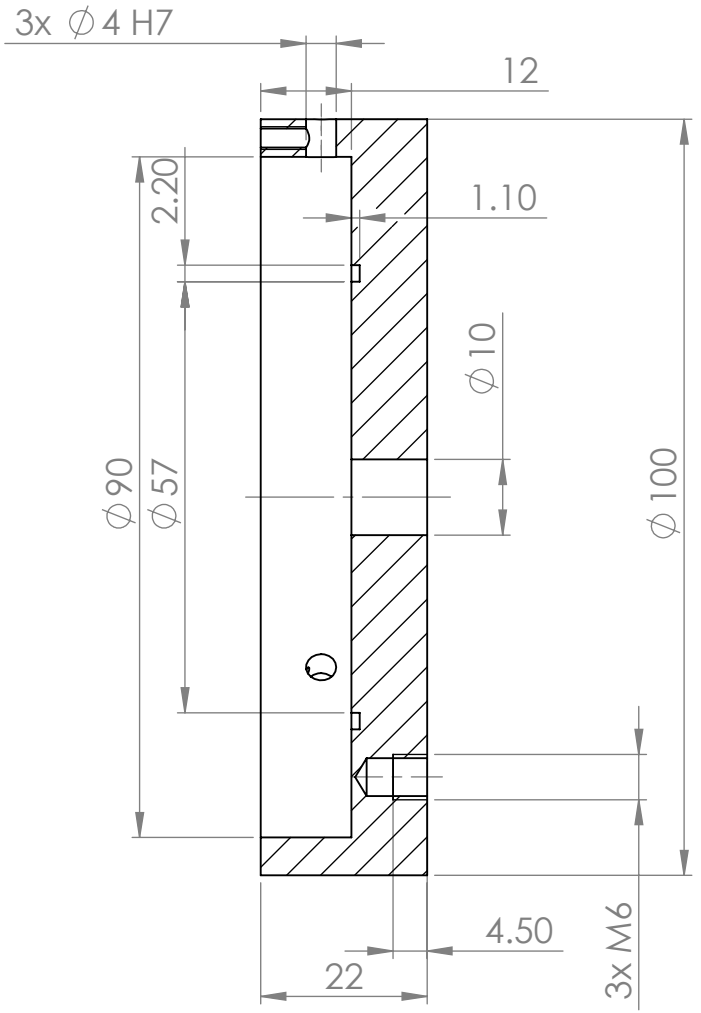

SCHNITT A-A
MAßSTAB 1 : 1

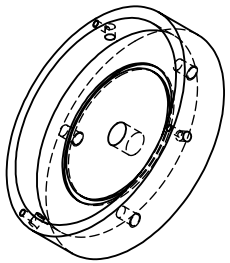

Kanten brechen 0,2x45°

Allgemeintoleranz nach SN EN 22768-1 mittel

Gezeichnet	GasDa
Datum	Freitag, 2. September 2016 07:58:51
Letzte Sicherung	Freitag, 2. September 2016 08:11:48
Stückzahl	**1**
Material:	Aluminium
Gewicht:	

ARTORG Forschungszentrum

UNIVERSITÄT BERN

Projektnummer: **1303**

C-Patch Testing Setup

Benennung: Bajonett_Patch

A4

Massstab: 1:1

Blatt 1 von 1

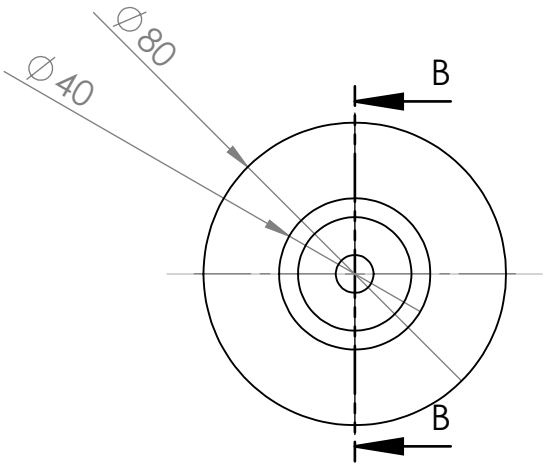

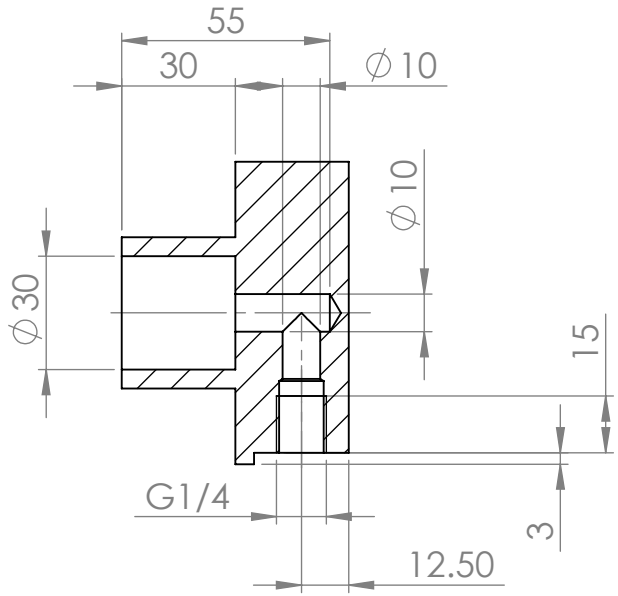

SCHNITT B-B

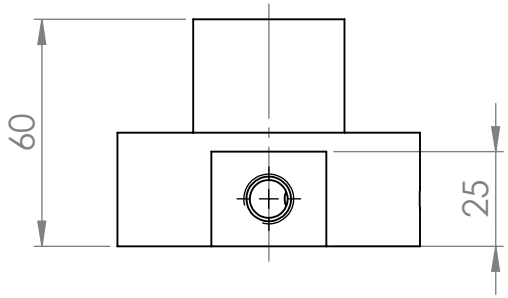

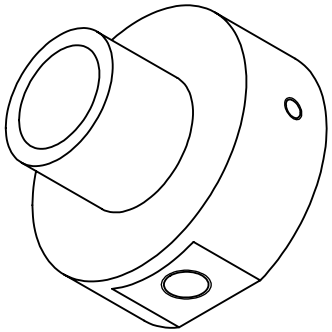

Kanten brechen 0,2x45°

Allgemeintoleranz nach SN EN 22768-1 mittel

Gezeichnet	GasDa
Datum	Freitag, 2. September 2016 08:25:17
Letzte Sicherung	Freitag, 2. September 2016 08:31:12
Stückzahl	**1**
Material:	Aluminium
Gewicht:	

ARTORG Forschungszentrum

UNIVERSITÄT BERN

Projektnummer: **1303**

C-Patch Testing Setup

Benennung:
Base_Water_Columne

A4

Massstab: 1:1

Blatt 1 von 1

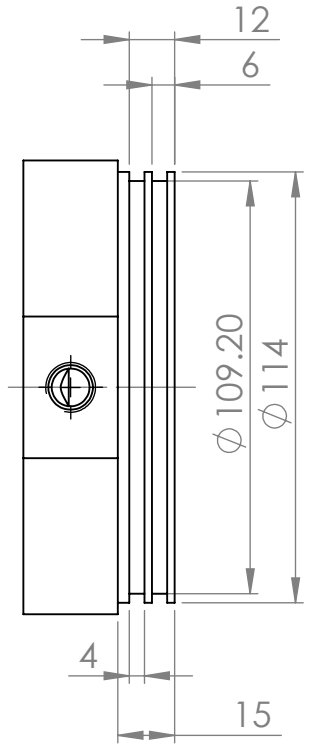

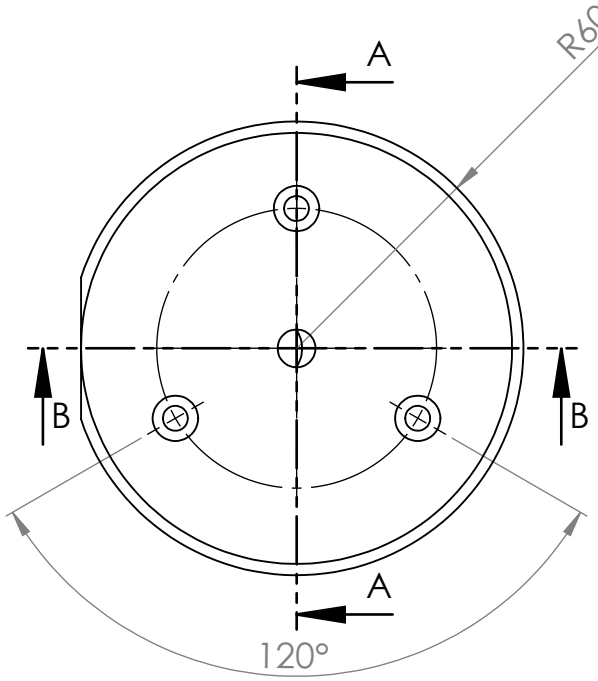

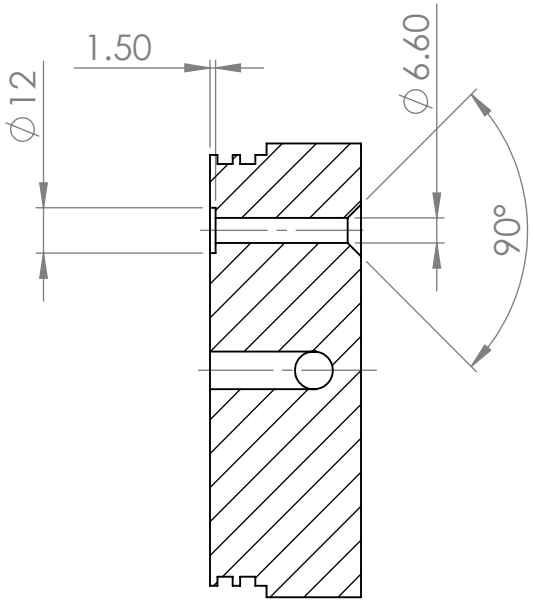

SCHNITT A-A

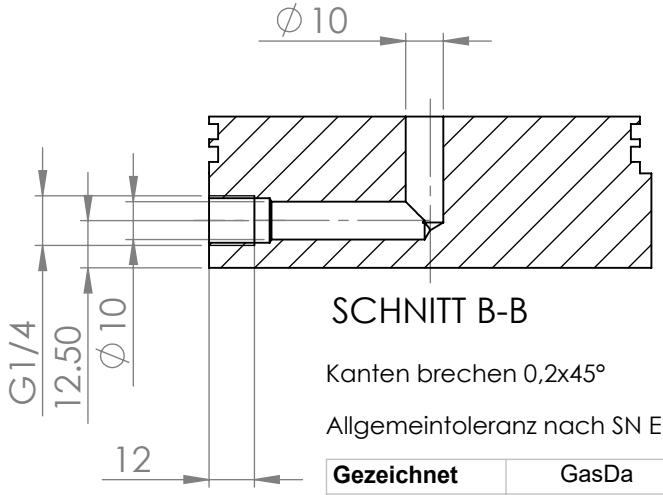

SCHNITT B-B

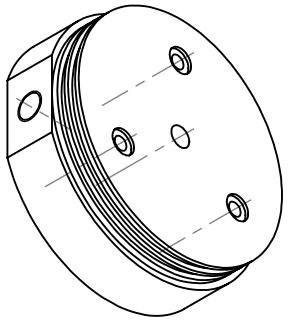

Kanten brechen 0,2x45°

Allgemeintoleranz nach SN EN 22768-1 mittel

Gezeichnet	GasDa
Datum	Freitag, 2. September 2016 08:11:58
Letzte Sicherung	Freitag, 2. September 2016 08:19:40
Stückzahl	**1**

Material: PVC

Gewicht:

ARTORG Forschungszentrum

UNIVERSITÄT BERN

Projektnummer: **1303**

C-Patch Testing Setup

Benennung: Groundflange_Patch

A4

Massstab: 1:1

Blatt 1 von 1

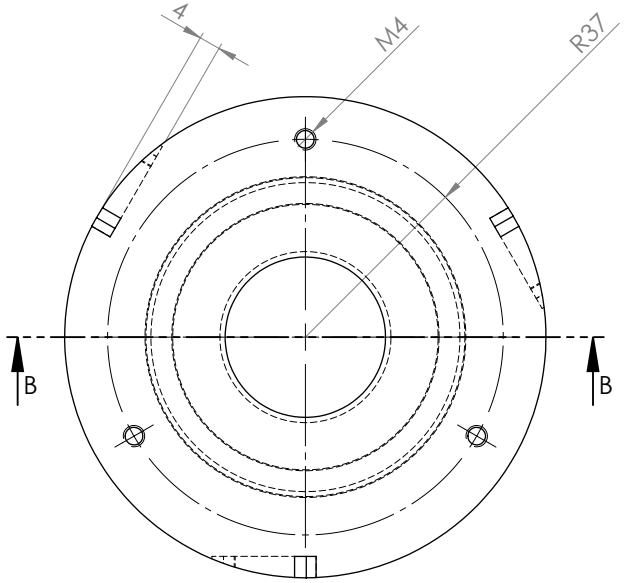

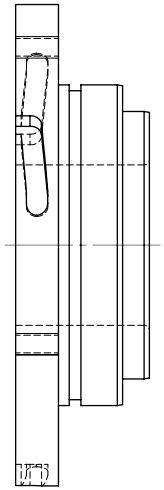

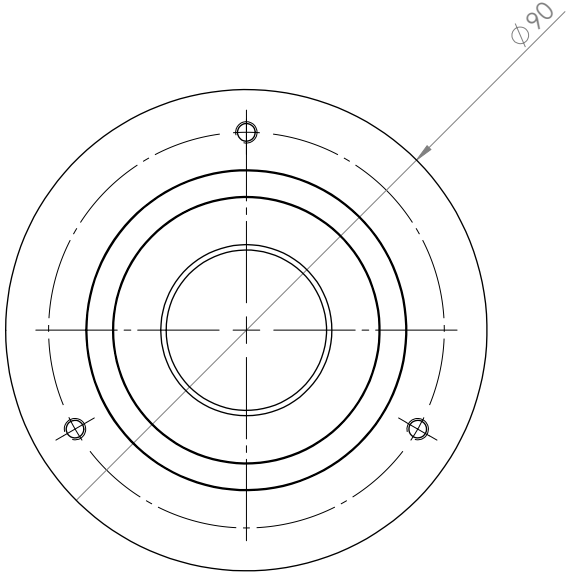

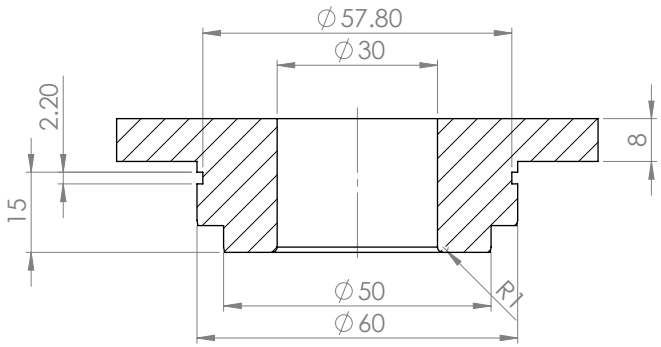

SCHNITT B-B

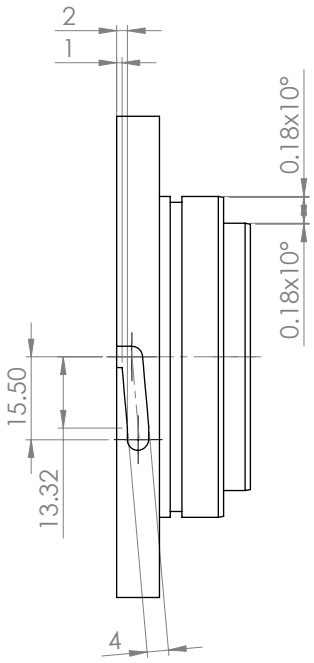

ARTORG Forschungszentrum

UNIVERSITÄT BERN

Gezeichnet	GasDa
Erstellt am	Freitag, 2. September 2016 07:36:58
Geändert am	Freitag, 2. September 2016 07:47:40
Stückzahl	1

Projektnummer: **1303**

C-Patch Testing Setup

Material: Aluminium

Benennung: Flange_Patch

A3

Massstab 1:1.5

Blatt 1 von 1

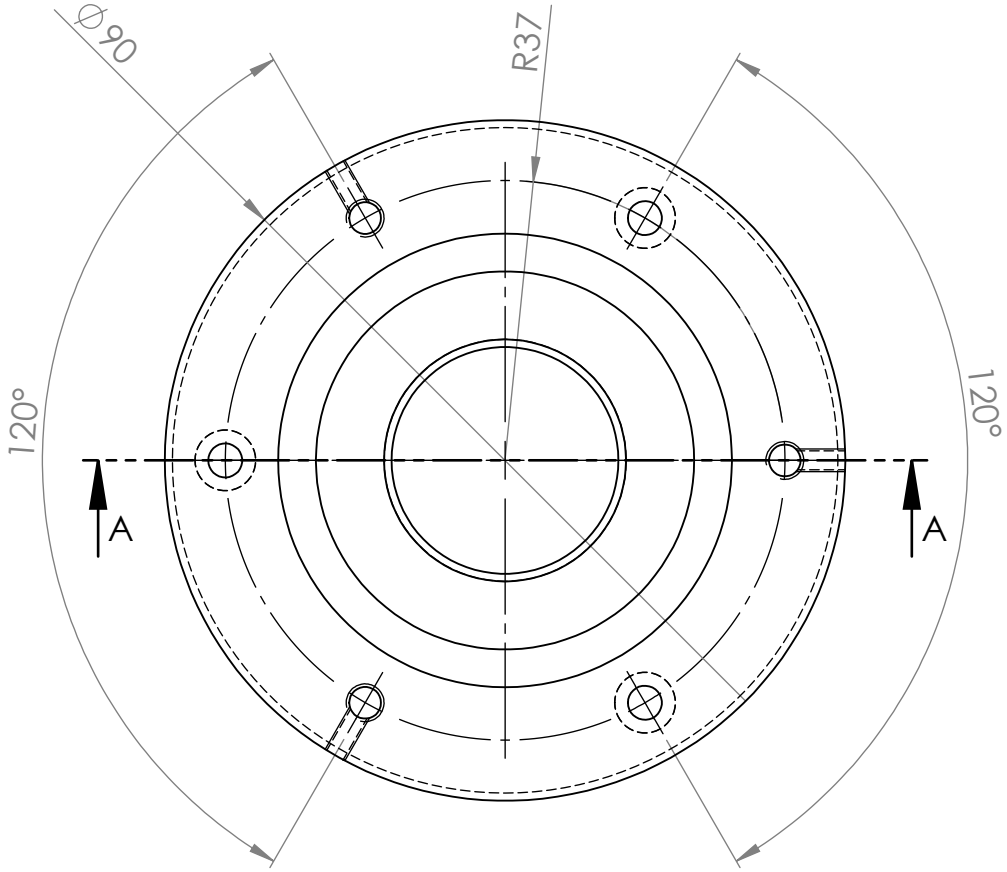

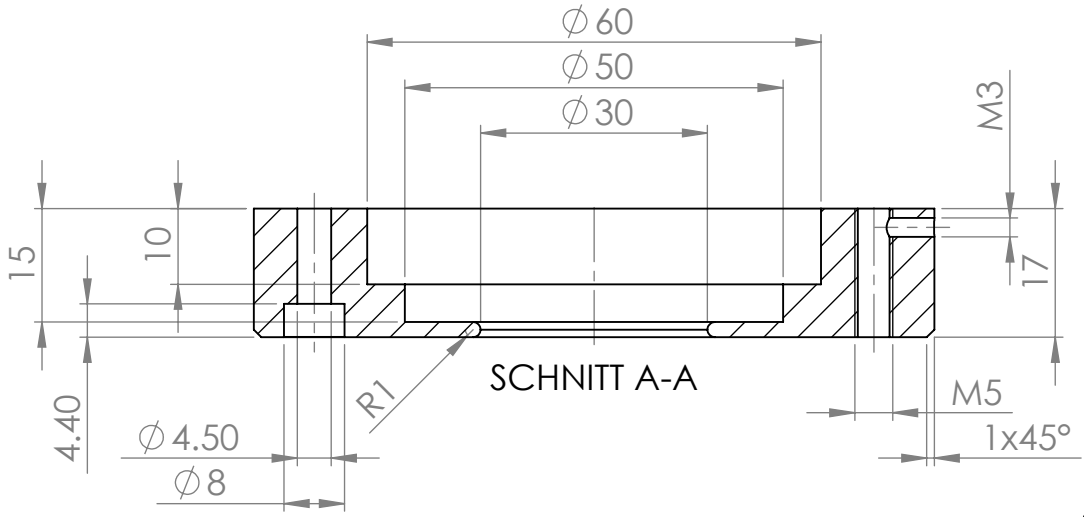

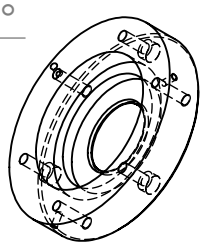

Kanten brechen 0,2x45°

Allgemeintoleranz nach SN EN 22768-1 mittel

ARTORG Forschungszentrum

UNIVERSITÄT BERN

Gezeichnet	GasDa
Datum	Freitag, 2. September 2016 07:45:52
Letzte Sicherung	Freitag, 2. September 2016 07:55:01
Stückzahl	1

Projektnummer: **1303**

C-Patch Testing Setup

Material: Aluminium

Benennung:

Flangering_Patch

A4

Gewicht:

Massstab: 2:1

Blatt 1 von 1

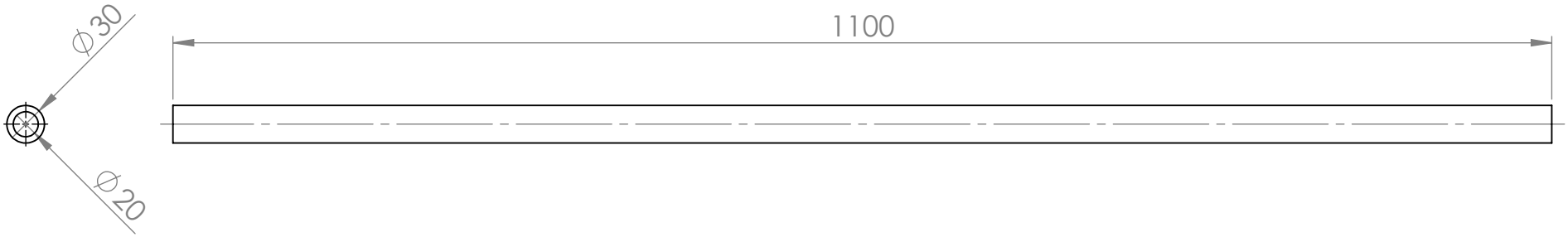

Kanten brechen 0,2x45°

Allgemeintoleranz nach SN EN 22768-1 mittel

Gezeichnet	GasDa
Datum	Freitag, 2. September 2016 08:21:53
Letzte Sicherung	Freitag, 2. September 2016 08:23:39
Stückzahl	**1**
Material:	Aluminium
Gewicht:	

ARTORG Forschungszentrum

UNIVERSITÄT BERN

Projektnummer: **1303**

C-Patch Testing Setup

Benennung: Tube_Water_Columne

A4

Massstab: 1:1

Blatt 1 von 1

Appendix C

Technical Drawings of the Rotary Device

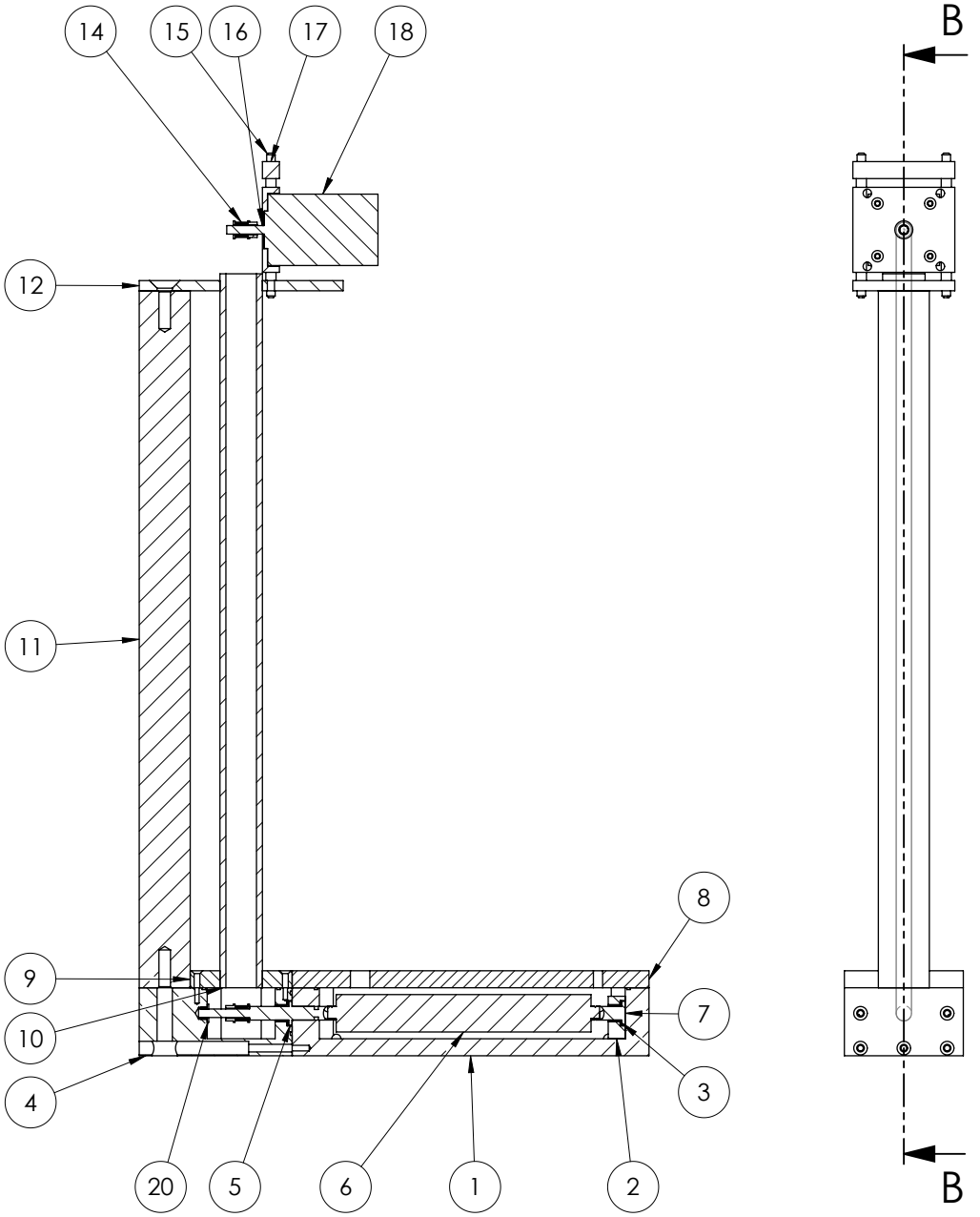

SCHNITT B-B

MAßSTAB 1 : 3

POS-NR.	BENENNUNG	MENGE
1	02_Cylinderchamber	1
2	03_Cylindersupport	1
3	14_Bearring	2
4	07_Axischamber	1
5	08_Axis	1
6	04_Cylinder	1
7	06_Cylinderaxis	1
8	05_Cylindercover	1
9	09_Axischambercover	1
10	10_Axispipe	1
11	12_Item_Profile	1
12	13_Moterplate	1
13	Teil1^00_ASM_Cylinder_Ratation_Box	1
14	16_Gear	2
15	20_Guiding	2
16	19_Motorfix	1
17	21_Guiding_Bridge	1
18	18_Motor	1
19	20_Cylinderwindow	2
20	22_Bearring_Small	1

ARTORG Forschungszentrum

UNIVERSITÄT BERN

Gezeichnet	GasDa
Erstellt am	Donnerstag, 19. April 2018 15:37:50
Geändert am	Donnerstag, 19. Juli 2018 10:04:48
Stückzahl	1

Material:

Projektnummer: **1409**

Jelly_Fish

Benennung:

00_ASM_Cylinder_Rotation_Box

A3

Massstab 1:3

Blatt 1 von 1

Appendix D

Additional Images of Rotary Test Results

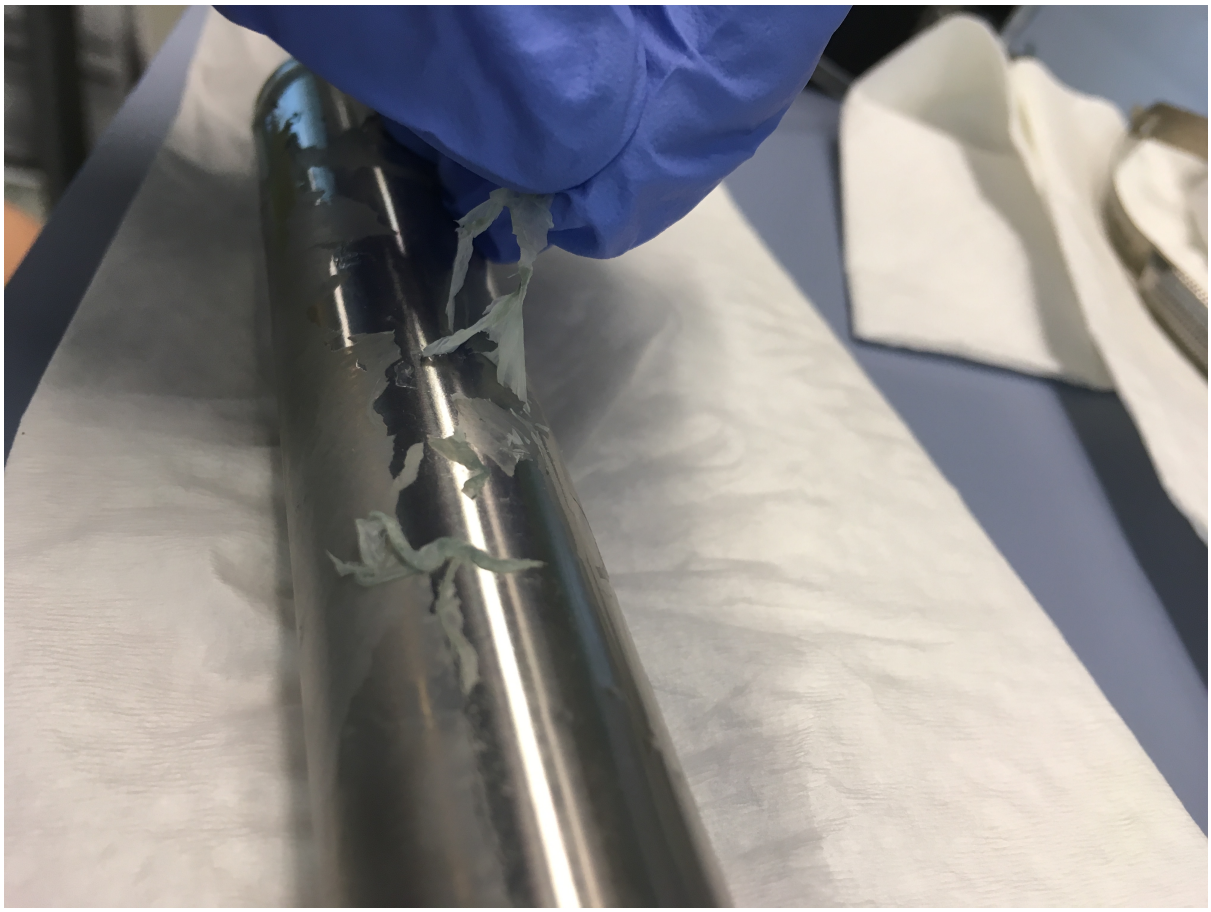

Fig. 4.1: *Material structure of Rotary Test 2; the stainless steel cylinder coated in silicon*

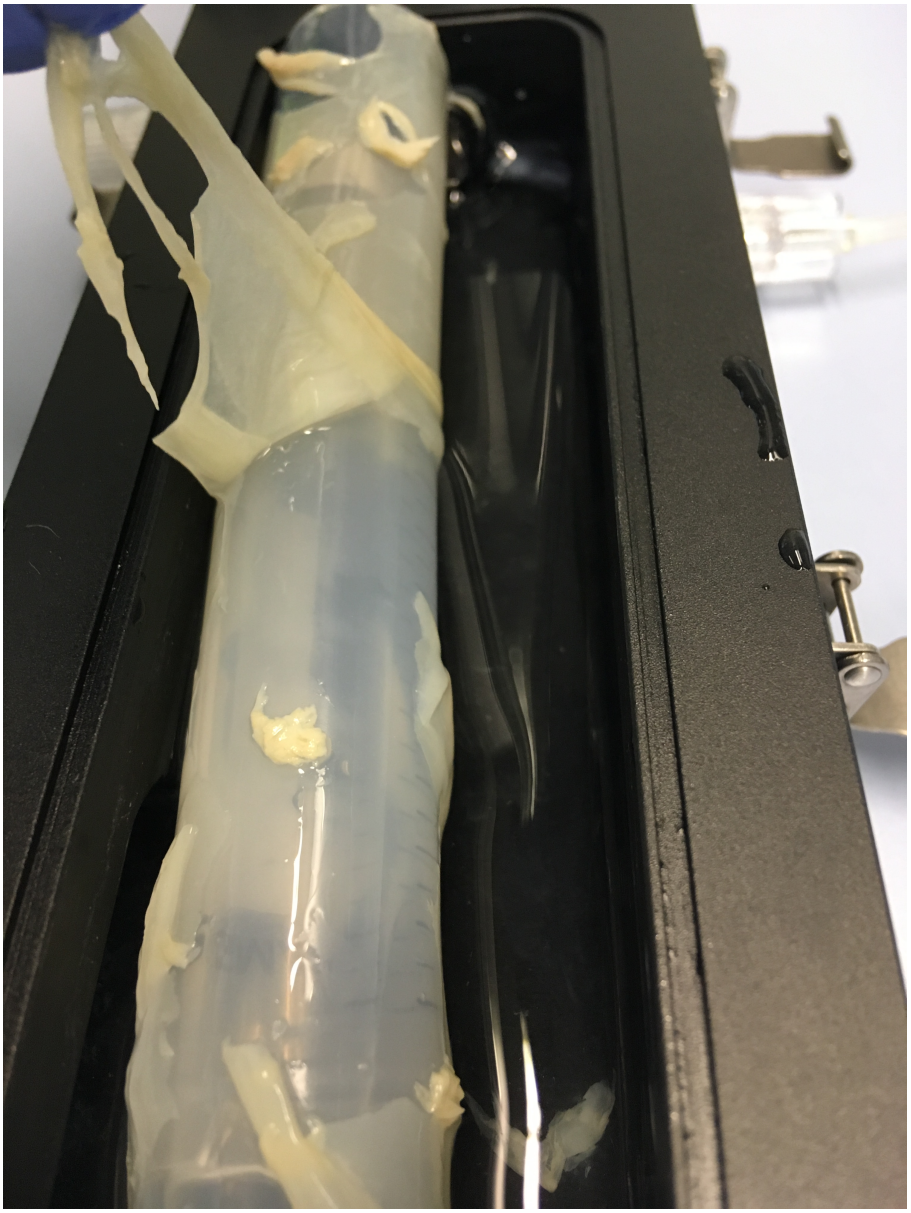

Fig. 4.2: *Material structure of Rotary Test 4; a silicon tube*

Appendix E

Quick Feasibility Test for Submersed Air-Permeable Tube

A quick test has been conducted to discover the feasibility of growing a BC tube on an air-permeable tube submersed in medium. A silicon tube (D6x1.5mm, Maagtechnic AG, Füllinsdorf, Switzerland). The tube was completely submersed inside the medium, within a Petri dish with a diameter of 100 mm.

The Petri dish was modified to include holes to allow for a tube to go in and out. The silicon tube was pulled through the holes and secured with medical epoxy adhesive (Loctite Hysol M-31CL Medical Device Epoxy Adhesive, Henkel AG & Company, Düsseldorf, Germany). The dish was then cleaned with ethanol and filled to the very top with medium (60 ml of medium). 6 mL of inoculum was added. This inoculum was gathered from patches from previous tests and multiplied in a shaker with medium for two days.

The dish was closed and cultured for five days under ambient conditions. The silicon tube was connected to an oxygen supply (70% oxygen) at 1 bar, and clamped shut on the other end. The clamping force was enough to keep air from blowing out, but a small airflow was possible. This would allow for a slow airflow within the tube, refreshing the oxygen levels.

Figure 5.1. Cellulose grew around the silicon tube, and on top of the medium. The top patch

Fig. 5.1: *The BC tube around the silicon tube after 6 days of culturing submersed in medium in a Petri dish. The surface patch has merged with the tube growing around the silicon*

merged together with the tube, while the tube had not been placed low enough in the medium. Air bubbles escaped trough the silicon tube, making the tubular BC very inhomogeneous and brittle. The tube could be removed from the silicon, but broke after cooking in distilled water.

Bibliography

[1] Bach, D. S. (2009). Echo/doppler evaluation of hemodynamics after aortic valve replacement. *JACC: Cardiovascular Imaging*, 33(3):296–304.

[2] Backdahl, H., Bodin, A., Helenius, G., Nannmark, U., Johansson, B., Risberg, B., and Gatenholm, P. (2006). Mechanical properties of bacterial cellulose and interactions with smooth muscle cells. *Biomaterials*, 27(9):2141–2149.

[3] Bodin, A., Backdahl, H., Fink, H., Gustafsson, L., Risberg, B., and Gatenholm, P. (2006a). Influence of cultivation conditions on mechanical and morphological properties of bacterial cellulose tubes. 97(2):425–34.

[4] Bodin, A., Bäckdahl, H., gustafsson, L., risberg, B., and Gatenholm, P. (2006b). Manufacturing and characterization of bacterial cellulose tubes using two different fermentation techniques. *Modern Multidisciplinary Applied Microbiology*.

[5] Bodin, A., Bharadwaj, S., Wu, S., Gatenholm, P., Atala, A., and Zhang, Y. (2010). Tissue engineered conduit using urine-derived stem cells seeded bacterial cellulose polymer in urinary reconstruction and diversion. *Biomaterials*, 31(34):8889–8901.

[6] Buerzle, W., Haller, C., Jabareen, M., Egger, J., Mallik, A., Ochsenbein-Koelble, N., Ehrbar, M., and Mazza, E. (2013). Multiaxial mechanical behavior of human fetal membranes and its relationship to microstructure. *Biomechanics and Modeling in Mechanobiology*, 12(4):747–762.

[7] Chanliaud, E., Burrows, K., Jeronimidis, G., and Gidley., M. (2002). Mechanical properties of primary plant cell wall analogues. *Planta*, 251(6):989–96.

[8] Chawla, P., Bajaj, I., Survase, S., and Singhal, R. (2009). Microbial cellulose: fermentative production and applications. *Food technology and biotechnology*, 47(2):107–124.

[9] Choi, Y., Hyde, K., and Ho, W. (1990). Single spore isolation of fungi. *fungal diversity*, 3:29–38.

[10] Costa, A. F. S., Almeida, F. C. G., Vinhas, G. M., and Sarubbo, L. A. (2017). Production of bacterial cellulose by gluconacetobacter hansenii using corn steep liquor as nutrient sources. *Frontiers in Microbiology*, 8:Article 2027.

[11] Czaja, W., Krystynowicz, A., Bielecki, S., and Brown, R. (2006). Microbial cellulose—the natural power to heal wounds. *Biomaterials*, 27(2):145–151.

[12] Czaja, W., Young, D., Kawecki, M., and jr., R. B. (2007). The future prospects of microbial cellulose in biomedical applications. *Biomacromolecules*, 8(1):1–12.

[13] Dahman, Y., Jayasuriya, K. E., and Kalis, M. (2010). Potential of biocellulose nanofibers production from agricultural renewable resources: Preliminary study. *Applied Biochemistry and Biotechnology*, 162:1647–1659.

[14] Dasi, L. P., Simon, H. A., Sucosky, P., and Yoganathan, A. P. (2009). Fluid mechanics of artificial heart valves. *Clinical and Experimental Pharmacology and Physiology*, 36(2):225–237.

[15] Dutton, J. (1991). Coralline hydroxyapatite as an ocular implant. *ophthalmology*, 98(3):370–7.

[16] Dvir, D., Bourguignon, T., Otto, C. M., Hahn, R. T., Rosenhek, R., Webb, J. G., Treede, H., Sarano, M. E., Feldman, T., Wijeysundera, H. C., Topilsky, Y., Aupart, M., Reardon, M. J., Mackensen, G. B., Szeto, W. Y., Kornowski, R., Gammie, J. S., Yoganathan, A. P., Arbel, Y., Borger, M. A., Simonato, M., Reisman, M., Makkar, R. R., Abizaid, A., McCabe, J. M., Dahle, G., Aldea, G. S., Leipsic, J., Pibarot, P., Moat, N. E., Mack, M. J., Kappetein, A. P., and Leon, M. B. (2018). Standardized definition of structural valve degeneration for surgical and transcatheter bioprosthetic aortic valves. *Circulation*, 137:388–399.

[17] Elsheikh, A. and Anderson, K. (2005). Comparative study of corneal strip extensometry and inflation tests. *Journal of the Royal Society Interface*, 2(3):177–185.

[18] Esa, F., Tasirin, S. M., and Abd.Rahman, N. (2014). Overview of bacterial cellulose production and application. *International Conference on Agricultural and Food Engineering*, 2(2):113–119.

[19] Esguerra, M., Fink, H., Laschke, M., Delbro, D., Jeppsson, A., Gatenholm, P., Menger, M., and Risberg, B. (2002). Intravital fluorescent microscopic evaluation of bacterial cellulose as scaffold for vascular grafts. *Journal of Biomedical Materials Research Part A*, 93(1):140–9.

[20] et al., R. N. (2014). Aha/acc guideline for the management of patients with valvular heart disease. *The Journal of thoracic and cardiovascular surgery*, 129:000–000.

[21] Fang, B., Wan, Y., Tang, T., Gao, C., and Dai, K. (2009). Proliferation and osteoblastic differentiation of human bone marrow stromal cells on hydroxyapatite - bacterial cellulse nanocomposite scaffolds. *Tissue engineering part A*, 15(5):1091–8.

[22] Fernando, T., Commeaux, S., and Troncoso, O. P. (2012). Biocompatibility of bacterial cellulose based biomaterials. *Journal of Functional Biomaterials*, 3(4):864–878.

[23] Fioretta, E., Dijkman, P., Emmert, M., and Hoerstrup, S. (2017). The future of heart valve replacement: recent developments and translational challenges for heart valve tissue engineering. *Journal of tissue engineering and regenerative medicine*, 12(1):e323–e335.

[24] Gao, X., Shi, Z., Kuśmierczyk, P., Liu, C., Yang, G., Sevostinov, I., and V.Silberschmidt, V. (2016). Time-dependent rheological behaviour of bacterial cellulose hydrogel. *Materials Science and Engineering: C*, 58:153–159.

[25] Goncalves, S., Padrao, J., Rodrigues, I., Silva, J., Sencadas, V., Lanceros-Mendez, S., Girao, H., Dourado, F., and Rodrigues, L. (2015). Bacterial cellulose as a support for the growth of retinal pigment epithelium. *biomacromolecules*, 16(4):1341–51.

[26] Grande, C., Torres, F., Gomez, C., Troncoso, O., Canet-Ferrer, J., and Martinez-Pastor, J. (2009). Morphological characterisation of bacterial cellulose-starch nanocomposites. *Polymers and Polymer composites*, 16:181–185.

[27] Hasler, D. (2017). Experimental investigation of the three-dimensional flow field in the vicinity of aortic valve prostheses (ph.d thesis). *University of Bern, Switzerland*.

[28] Hassard, F., Biddle, J., Cartmell, E., Jefferson, B., Tyrell, S., and Stephenson, T. (2015). Rotating biological contactors for wastewater treatment – a review. *Process safety and environmental protection*, 94:285–306.

[29] Hayashida, K., Kanda, K., and et al., H. Y. (2007). Development of an in vivo tissue-engineered, autologous heart valve (the biovalve): preparation of a prototype model. *Journal of Thoracic Cardiovascular Surgery*, 134(1):152–9.

[30] Helenius, G., Backdahl, H., Bodin, A., Nannmark, U., Gatenholm, P., and Risberg, B. (2006). In vivo biocompatibility of bacterial cellulose. *Journal of Biomedical Materials Research Part A*, 76A(2):431–438.

[31] Ho, S. (2009). Structure and anatomy of the aortic root. *European Journal of Echocardiography*, 10(1):I3–10.

[32] Hoerstrup, S., Sodian, R., Daebritz, S., Wang, J., and et al., E. B. (2000). Functional living trileaflet heart valves grown in vitro. *Circulation*, 102(19 suppl 3):III44–9.

[33] hutmacher, D., schantz, J., Lam, C., Tan, K., and Lim, T. (2007). State of the art and future directions of scaffold-based bone engineering from a biomaterials perspective. *Journal of Tissue engineering and regenerative medicine*, 1(4):245–60.

[34] Kim, Y.-J., Kim, J.-N., jung Wee, Y., hee Park, D., and Ryu, H.-W. (2007). Bacterial cellulose production by gluconacetobacter sp. rky5 in a rotary biofilm contactor. 137-140(1-12):529–37.

[Klabunde] Klabunde, R. E. *Cardiovascular Physiology Concepts*. Number 9781451113846. Lippincott Williams and Wilkins, 2nd edition.

[36] Klemm, D., Schumann, D., Udhardt, U., and Marsch, S. (2001). Bacterial synthesized cellulose: artificial blood vessels for microsurgery. *Progress in Polymer science*, 26(9):1561–1603.

[37] Krystynowicz, A., Czaja, W., Wiktorowska-Jezierska, A., Goncalves-Miskiewicz, M., Turkiewicz, M., and Bielecki, S. (2002). Factors affecting the yield and properties of bacterial cellulose. *Journal of Industrial Microbiology and Biotechnology*, 29(4):189–95.

[38] Lin, S., Hsieh, S., Chen, K., Demirci, A., and Cheng, K. (2014). Semi-continuous bacterial cellulose production in a rotating kisc bioreactor and its materials properties analysis. *Cellulose*, 21(1):835–844.

[39] Loukas, M., Bilinsky, E., Bilinsky, S., Blaak, C., Tubbs, R., and Anderson, R. (2014). The anatomy of the aortic root. *Clinical Anatomy*, 27(5):748–56.

[40] M. Nordin, V. F. (2001). *Basic Biomechanics of the Musculoskeletal System*. 3rd edition.

[41] Marieb, E. N. and Hoehn, K. (2013). *Human Anatomy and Physiology*. Number 9780321743268. Pearson, 9th edition.

[42] Masoumi, N., Annabi, N., Assmann, A., Larson, B. L., Hjortnaes, J., Alemdar, N., Kharaziha, M., Manning, K. B., Mayer, J., and Khademhosseini, A. (2014). Tri-layered elastomeric scaffolds for engineering heart valve leaflets. *Biomaterials*, 35(27):7774–85.

[43] Mendelson, K. and Schoen, F. J. (2006). Heart valve tissue engineering: Concepts, approaches, progress, and challenges. *Annals of Biomedical Engineering*, 34(12):1799–1819.

[44] Mendes, P., Rahal, S., Pereira, O., Fabris, V., Lenharo, S., Lima, J., and Alvarenga, F. (2009). In vivo and in vitro evaluation of an acetobacter xylinum synthesized microbial cellulose membrane intended for guided tissue repair. *Planta*, 51(1):12.

[45] M.Lee, Fung, Y., Shabetai, R., and Lewinter, M. (1987). Biaxial mechanical properties of human pericardium and canine comparisons. *American Journal of Physiology*, 253(1 Pt 2):H75–82.

[46] Nienhaus, A. G. (2017). Bacterial cellulose-based patches for heart surgery - investigation of culturing conditions and material characterization. *Msc. Thesis*.

[47] Norhayati, P. (2009). Rotary discs reactor for enhanced production of microbial cellulose. *Master thesis*.

[48] N.Petersen and P.Gatenholm (2011). Bacterial cellulose-based materials and medical devices: current state and perspectives. *Applied Microbiology and Biotechnology*, 91(5):1277–86.

[49] Park, S., Kim, J., and Suh, H. (2004). Evaluation of antibiotic-loaded collagen-hyaluronic acid matrix as a skin substitute. *Biomaterials*, 25(17):3689–98.

[50] Pibarot, P. and Dumesnil, J. G. (2009). Prosthetic heart valves: Selection of the optimal prosthesis and long-term management. *Circulation*, 119(7):1034–48.

[51] Picard-Deland, M., Ruel, J., Galbraith, T., Tremblay, C., Kawecki, F., Germain, L., and Auger, F. A. (2016). Tissue-engineered tubular heart valves combining a novel precontraction phase with the self-assembly method. *Annals of Biomedical Engineering*, 45(2):427–438.

[52] Rangaswamy, B., Vanitha, K., and Hungund, B. S. (2015). Microbial cellulose production from bacteria isolated from rotten fruit. *international journal of polymer science*, 2015(2):1–8.

[53] Sacks, M. S., Schoen, F. J., , and Jr., J. E. M. (2009). Bioengineering challenges for heart valve tissue engineering. *Annual Review of Biomedical Engineering*, 11:289–313.

[54] Saikrishnan, N., Kumar, G., Sawaya, F., Lerakis, S., and Yoganathan, A. (2014). Accurate assessment of aortic stenosis: a review of diagnostic modalities and hemodynamics. *Circulation*, 129(2):244–53.

[55] Schumann, D., Wippermann, J., Klemm, D., Koth, D., Kramer, F., Kosmehl, H., Salehi-Gelani, S., and Wahlers, T. (2009). Artificial vascular implants from bacterial cellulose: preliminary results of small arterial substitutes. *Cellulose*, 16(5):877–885.

[56] Serafica, G. (1997). Production of bacterial cellulose using a rotating disk film bioreactor by acetobacter xylinum. *Ph.D. Thesis*, 84(1):533–538.

[57] Smeenk, M. (2018a). Feasibility of bacterial cellulose as a biomaterial for heart valve prosthetics. *Literature Research for Master Thesis*.

[58] Smeenk, M. (2018b). Feasibility study into bacterial cellulose heart valves. *Master Internship Report*.

[59] Svensson, A., Nicklasson, E., Harrah, T., Panilaitis, B., Kaplan, D., Brittberg, M., and Gatenholm, P. (2005). Bacterial cellulose as a potential scaffold for tissue engineering of cartilage. *Biomaterials*, 26(4):419–31.

[60] Thielicke, W. (2014). The flapping flight of birds - analysis and application. *PhD Thesis*.

[61] Thielicke, W. and Stamhuis, E. (2014). Pivlab – towards user-friendly, affordable and accurate digital particle image velocimetry in matlab. *ournal of Open Research Software*.

[62] Tillquist, M. and Maddox, T. (2011). Cardiac crossroads: deciding between mechanical or bioprosthetic heart valve replacement. *Patient preference and adherence*, 5:91–99.

[63] Vesely, I. (2005). Heart valve tissue engineering. *Circulation Research*, 97:743–755.

[64] Winkler, B., Grapow, M., Eckstein, F., Ferrari, A., Poulikakos, D., Botan, S., Fischer, M., and Lendenmann, T. (2015). Artificial vascular graft. *WO 2015040139 A1*.

[65] Wippermann, J., Schumann, D., Klemm, D., Kosmehl, H., Salehi-Gelani, S., and Wahlers, T. (2009). Preliminary results of small arterial substitute performed with a new cylindrical biomaterial composed of bacterial cellulose. *European Journal of Vascular and Endovascular Surgery*, 37(5):592–596.

[66] Wurdinger, J., Marsch, S., Udhardt, U., and Schumann, H. (2000). Basyc (bacterial synthesized cellulose)-the vitalization of a microvessel-prosthesis in the rat. *Microsurgery*, 20:268.

[67] Yamanaka, S., Watanabe, K., Kitamura, N., Iguchi, M., Mitsuhashi, S., Nishi, Y., and Uryu, M. (1989). The structure and mechanical properties of sheets prepared from bacterial cellulose. *Journal of Materials science*, 24(9):3141.

[68] Zahedmanesh, H., Mackle, J. N., Sellborn, A., Drotz, K., Bodin, A., Gatenholm, P., and Lally, C. (2010). Bacterial cellulose as a potential vascular graft: Mechanical characterization and constitutive model development. *Journal of Biomedical Materials Research B: Applied Biomaterials*, 97(1):105–13.